Title

Kinetics of D/H isotope fractionation between molecular hydrogen and water

Authors

Pester, Nicholas J
Conrad, Mark E
Knauss, Kevin G
et al.

Publication Date

2018-12-01

DOI

10.1016/j.gca.2018.09.015

Peer reviewed

Available online at www.sciencedirect.com

ScienceDirect

Geochimica et Cosmochimica Acta 242 (2018) 191–212

Geochimica et Cosmochimica Acta

www.elsevier.com/locate/gca

Kinetics of D/H isotope fractionation between molecular hydrogen and water

Nicholas J. Pester [a,b,*], Mark E. Conrad [a], Kevin G. Knauss [a], Donald J. DePaolo [a,b]

[a] Earth and Environmental Sciences Area, Lawrence Berkeley National Laboratory, Berkeley, CA 94720, USA
[b] Department of Earth and Planetary Science, University of California, Berkeley, Berkeley, CA 94720, USA

Received 13 March 2018; accepted in revised form 12 September 2018; Available online 24 September 2018

Abstract

At equilibrium, the D/H isotope fractionation factor between H_2 and H_2O ($\alpha_{H2O\text{-}H2(eq)}$) is a sensitive indicator of temperature, and has been used as a geothermometer for natural springs and gas discharges. However, δD_{H2} measured in spring waters may underestimate subsurface temperatures of origin due to partial isotopic re-equilibration during ascent and cooling. We present new experimental data on the kinetics of D–H exchange for H_2 dissolved in liquid water at temperatures below 100 °C. Comparing these results with published exchange rates obtained from gas phase experiments (100–400 °C), we derive a consistent activation energy of 52 kJ/mol, and the following rate expressions;

$$\ln k = 9.186 - 6298/T \quad \text{and} \quad k_1 = 9764.61\ [H_2O]\ e^{-6298/T}$$

where T is absolute temperature (K), k is the universal rate constant ([L/mol]/hr), and k_1 is a pseudo-first-order constant (hr^{-1}) applicable to water-dominated terrestrial systems by constraining $[H_2O]$ as the density of H_2O (in mol/L) at the P-T of interest. The density-dependent rate constant accounts for the kinetic disparity of D–H exchange with H_2 when dissolved in liquid H_2O relative to a gas/steam phase, exemplified by $1/k_1$ at 100 °C of ~2 days in liquid, versus ~7 yrs in saturated steam. This difference may explain the high variability of δD_{H2} observed in fumarolic gases. Fluids convecting in the crust frequently reach $T > 225$ °C, where isotopic equilibrium is rapidly attained (<1 hr). We compare fractionation factors measured in natural fluids (α_{OBS}) with values expected for equilibrium at the T of acquisition. Where these values differ, we use kinetic models to estimate cooling rates during upward advection that account for the observed disequilibrium. Models fit to fluids from Yellowstone Park and the Lost City (deep-sea) vent field, both recovered at ~90 °C, require respective transit times of ~7 hrs and ~11 days between higher temperature reaction zones and the surface. Using estimates of subsurface depths of origin, however, suggests similar mean fluid flow rates (10 s of meters/hr). Additional complications must be considered when interpreting the δD_{H2} of lower-temperature effluent. When applied to data from deep-sea hydrothermal systems, our kinetic models indicate microbial catalysis accelerates D–H exchange once fluids cool below ~60 °C. The H_2 measured in both continental alkaline springs and fracture fluids from Precambrian shield rock is likely produced at $T < 100$ °C, through processes such as serpentinization. In these settings, δD_{H2} values appear closer to equilibrium with H_2O than those from geothermal systems. Considering kinetic isotope effects may yield H_2 that is out of equilibrium when generated at lower temperatures, we calculate maximum (isothermal) times to apparent isotopic equilibrium of 1.3 yrs at 50 °C, 9 yrs at 25 °C, and 35 yrs at 10 °C. A similar calculation applied to Antarctic brines (−13 °C), where measured δD_{H2} is far from equilibrium, yields ~350 yrs. This time is shorter than the fluids have been isolated (2.8 ka), suggesting kinetic isotope effects associated with H_2 destruction or loss via diffusion may also be possible.

Keywords: Hydrogen isotopes; Isotope exchange kinetics; Hydrothermal system; Lost City; Volcanic gas; Serpentinization; Microbial catalysis; Geothermometer

* Corresponding author at: Present address: Department of Earth and Planetary Science, University of California, Berkeley, CA 94720, USA.
E-mail address: njpester@berkeley.edu (N.J. Pester).

https://doi.org/10.1016/j.gca.2018.09.015
0016-7037/

1. INTRODUCTION

Molecular hydrogen (H_2) is a common component of crustal fluids and discharges, where water has reacted with reduced (usually Fe-bearing) minerals. The concentration of H_2 in volcanic gases and hydrothermal fluids is a function of both temperature (T) and the oxidation state of coexisting mineral assemblages (D'Amore and Panichi, 1980; Kishima and Sakai, 1984; Giggenbach, 1987; Kishima, 1989; Seyfried et al., 1991; Giggenbach, 1997; Chiodini and Marini, 1998). Similarly, mafic silicate minerals are unstable in the presence of H_2O at $T < \sim$400 °C, and partial oxidation of the Fe(II) component is capable of producing significant amounts of H_2 during serpentinization (Berndt et al., 1996a; Sleep et al., 2004; Seyfried et al., 2007; Mayhew et al., 2013; Klein et al., 2015; McCollom et al., 2016). Serpentinization is the most likely source of H_2-rich fluids/gases recovered from alkaline springs, ophiolites, and continental wells at relatively low temperatures (<∼60 °C) (Barnes et al., 1978; Neal and Stanger, 1983; Coveney et al., 1987; Abrajano et al., 1990; Sherwood Lollar et al., 1993b; Kelley et al., 2005).

Hydrogen concentrations measured in natural solutions generally give ambiguous information regarding temperatures of origin or formation. However, isotope fractionation between H_2 and H_2O is not concentration-dependent, and is a less equivocal indicator of temperature. The heavy stable isotope of hydrogen (^2H, ∼0.015 % of natural abundance) is commonly referred to as deuterium (or D), and the D/H isotope fractionation factor (alpha) between coexisting H_2O and H_2 is written as;

$$\alpha_{H2O-H2} = \frac{[D/H]_{H2O}}{[D/H]_{H2}} = \frac{\delta D_{H2O} + 10^3}{\delta D_{H2} + 10^3} \quad (1)$$

where [D/H] is the atomic ratio of the heavy and light hydrogen isotopes for each species. In order to facilitate inter-laboratory comparison of results, laboratory measurements of isotopic ratios are usually reported relative to the measured value of an accepted standard (δ notation) such that, for example, $\delta D_{H2} = [([D/H]_{H2}/[D/H]_{standard}) - 1] * 10^3$ (Craig, 1961).

The fractionation factor at equilibrium, $\alpha_{H2O\text{-}H2(eq)}$, is highly sensitive to temperature (e.g., Friedman and O'Neil, 1977; Richet et al., 1977), and is therefore useful as a geothermometer, which saw early application to geothermal and fumarolic gases (Friedman, 1953; Arnason, 1977; Kiyosu, 1983; Mizutani, 1983; Lyon and Hulston, 1984), and also fault gases (Kita et al., 1980). Geothermometers based on fluid/gas chemistry are usually applied to solutions advected to the surface with the expectation that they provide information about subsurface processes that cannot be directly observed or sampled in-situ. This type of geothermometer therefore requires the elements or species involved to exhibit chemical or isotopic disequilibrium relative to the conditions measured at the surface, where the solution sample was acquired. For example, Fig. 1 plots the *measured* H_2O–H_2 fractionation factors (defined herein as α_{OBS}) against T measured at the point of sampling for a variety of geologic settings, and the field samples commonly have α_{OBS} values that deviate from the equilibrium curve in a manner that indicates the solution had previously experienced a higher T. This combined dataset also allows us to conclude that the kinetics of D–H exchange between H_2 and H_2O is rapid for $T >$ ∼300 °C. Therefore, beyond a minimum (apparent) T of formation, the amount of information to be gained from observed disequilibrium relies foremost on understanding the relevant reaction kinetics.

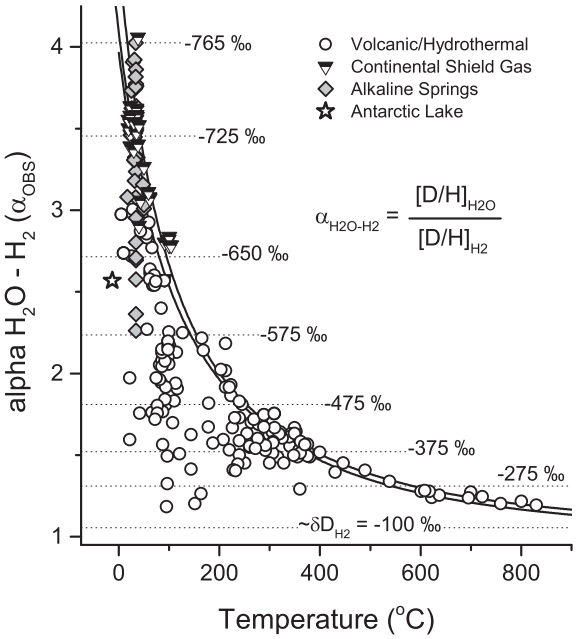

Fig. 1. Compendium of hydrogen isotope field data for H_2–H_2O compared with T-dependent equilibrium. Field data shows measured fractionation factor (α_{OBS}) vs. T measured during sample acquisition. Equilibrium range ($\alpha_{H2O\text{-}H2(eq)}$, solid curves) is defined from experimental and theoretical investigations (Bardo and Wolfsberg, 1976; Horibe and Craig, 1995; Richet et al., 1977; Suess, 1949). Representative values of δD_{H2} (calculated assuming $\delta D_{H2O} = -50$) are shown for reference. Alkaline springs/ophiolite data: Hakuba Happo, Japan (Suda et al., 2014); Dinaride ophiolite, Bosnia/Herzegovina (Etiope et al., 2017); Amik Basin, Turkey (Yuce et al., 2014); Semail ophiolite, Oman (Fritz et al., 1992; Miller et al., 2016; Neal and Stanger, 1983; Vacquand et al., 2018); Zambales ophiolite, Philippines (Abrajano et al., 1990; Sherwood Lollar et al., 2007; Vacquand et al., 2018). Zambales data are free gas emanations and δD_{H2O} and maximum measured T of nearby spring water are assumed (Cardace et al., 2015). Precambrian shield gases: Fennoscandian Shield, Finland (Kietäväinen et al., 2017), Gravberg, Sweden (Jeffrey and Kaplan, 1988), Canadian Shield (Sherwood Lollar et al., 2008; Sherwood Lollar et al., 2007), Witwatersrand Basin, South Africa (Onstott et al., 2006; Sherwood Lollar et al., 2007). Of shield gases, measured T only reported from South Africa, other values estimated using well depths and following geothermal gradient: 10 °C for top 500 m, then increasing 16 °C/km (Ahlbom et al., 1995; Jessop and Lewis, 1978; Juhlin et al., 1998; Komor et al., 1988; Marsic and Grundfelt, 2013). Datum from Lake Vida, Antarctica from Murray et al. (2012). See Figs. 8–10 for more detail and additional data references.

Surprisingly, few constraints exist on uncatalyzed rates of H_2–H_2O isotope exchange, especially for H_2 dissolved in liquid water. Using an experimental apparatus that

eliminates the need to account for gas–liquid (multiphase) exchange, we have therefore derived the D–H exchange rate for dissolved H_2 at three temperatures below 100 °C. These data may be used to help deduce residence or transit times for fluid movement in the crust, and they also provide an important basis for identifying and quantifying the extent to which microbial biomes catalyze D–H exchange with water. Furthermore, we use previously published data on gas-phase exchange rates (Lecluse and Robert, 1994) to infer a solution density dependence in the rate law. This formulation should serve to simplify the inclusion of H_2–H_2O isotope exchange kinetics in more complicated multiphase models that explore processes ranging from boiling in geothermal systems (Truesdell et al., 1977; Drummond and Ohmoto, 1985; Spycher and Reed, 1988) to the origin of water on Earth and elsewhere in the solar system (Lecluse and Robert, 1994; Robert et al., 2000; Genda and Ikoma, 2008; Niemann et al., 2010; Albertsson et al., 2014). Should better isotopic data be obtained by future space missions, the new rate relationships may also prove valuable in assessing the temperature of suspected subsurface oceans on icy satellites such as Enceladus, where H_2 has been measured in plumes of vapor and particulates jetting from cracks in the frozen outer shell (Hsu et al., 2015; Waite et al., 2009, 2017).

2. METHODS

2.1. Experimental design and protocol

The primary goal of this laboratory study was to observe the rate at which dissolved H_2 approaches isotopic equilibrium with H_2O at different temperatures. Starting reactants were grade 5 hydrogen gas, additionally filtered through a combined oxygen-moisture-hydrocarbon trap ($\delta D_{H2} = -107‰$ VSMOW), and deuterium-enriched H_2O ($\delta D_{H2O} \approx +5220‰$ VSMOW). The H_2 and H_2O were therefore initially far from isotopic equilibrium for any T of interest. The most important factor for the experimental design is that the dissolved H_2 remain undersaturated, and no gas phase (headspace) be allowed to exist or develop as a result of sample acquisition. The experiment was therefore carried out in a flexible gold reaction cell system, which is designed to monitor the time series progression of hydrothermal reactions at constant pressure (P) and T (Seyfried et al., 1979, 1987; Berndt et al., 1996b). Given all wetted parts consist of gold and titanium, this reactor is also the best option for avoiding effects of both surface catalysis and H_2 diffusion over the course of the experiment (Palmer and Drummond, 1986; Seward and Kishima, 1987; Lemke et al., 2009; Reeves et al., 2012).

This system consists of a flexible gold cell (~250 ml volume) with a passivated (oxidized) titanium head (closure) and sampling tube that is sealed within a steel pressure vessel (Fig. 2). This entire assembly is insulated within a rocking furnace, where desired temperature is maintained by proportional control microprocessors. The Ti sampling tube terminates external to the steel vessel/furnace, and is capped with a high-pressure Ti valve for extracting experimental solutions isolated in the gold cell. In order to control

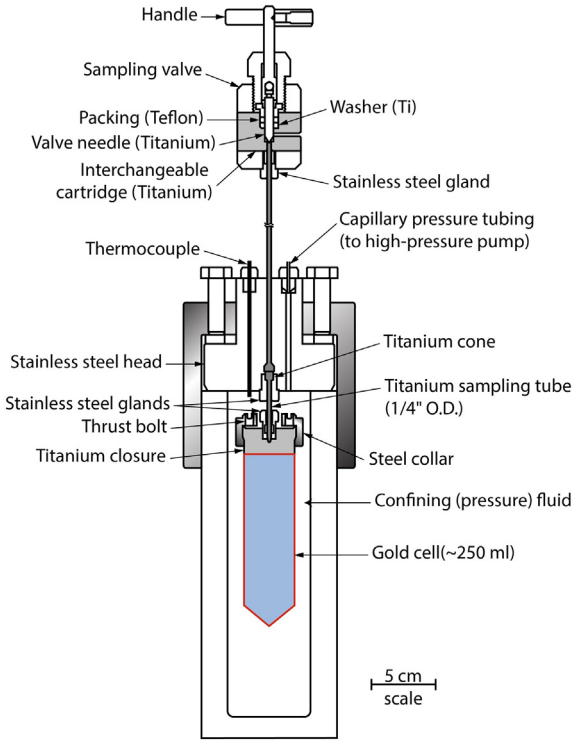

Fig. 2. Schematic representation of flexible gold reaction cell system used to determine kinetics of H_2–H_2O isotope exchange (see Section 2.1). Designed for hydrothermal experiments (all wetted parts are Au or Ti), time-series sampling of fluids in Au cell can be accomplished without a loss of system pressure (Seyfried et al., 1979, 1987). H_2 therefore remained fully dissolved over course of experiments.

system pressure, the void space within the steel vessel (external to the gold cell) is filled with distilled water, and open to a valved network of tubing that includes in-line strain gauge transducers and a high-pressure syringe pump. Because the gold reaction cell is flexible, the confining pressure in the steel vessel and that within the reaction cell are equivalent. The system therefore permits isobaric sampling by directing the syringe pump to maintain the desired confining pressure, while an aliquot of reactant fluid is expressed by (carefully) opening the Ti valve. Essentially, an equal volume of confining fluid is simultaneously added as sample fluid is being removed, and with each sample extracted (over the course of the experiment), the gold cell incrementally collapses, much like a tube of toothpaste. New fluid or gaseous reactants may similarly be introduced into the gold cell at any time (through the Ti valve) as long as the maximum capacity is not exceeded.

The experimental setup was as follows. The gold cell was filled near capacity with the spiked H_2O and sparged with grade 5 Ar gas for 45 mins to best eliminate other dissolved gases. The sparging tube was removed, and the flow of Ar was then routed through the titanium closure assembly (includes the valve and sampling tube and closure), which was loosely fitted into the gold cell. Prior to fully sealing the Ti closure, any remaining headspace in the cell was allowed to purge for another 15 min. The Au-Ti assembly

was then sealed into the steel vessel with a full complement of confining water, and the system was situated in the rocking furnace with a vertical orientation (i.e. the sampling tube pathway was vertical, same as the orientation shown in Fig. 2). Still at ambient *P-T*, a syringe was attached to the Ti sampling valve, the valve was opened, and additional confining water was pumped into the steel vessel until reactant water began to appear in the syringe. This signified that the majority of the remaining Ar headspace in the gold cell had been removed through the sampling tube. With the sampling valve then closed, the system was pressure tested at 500 bars over night, and no leaks were detected. Pressure was relieved to ambient, and a sufficiently large sample of reactant water was removed from the gold cell to make room for a charge of H_2 gas (~20 ml). Prior to adding the H_2, the system was stabilized at the initial experimental *T* of 97 °C in order to avoid ambiguous reaction progress during heating. With the apparatus still oriented vertically (cf. Fig. 2), the gas line from the H_2 tank was flushed prior to sealing in the (closed) Ti sampling valve, and was then pressurized to ~65 psig. Cell confining *P* was again balanced to ambient, the Ti valve then opened, and the system registered the tank pressure. The piston in the syringe pump was directed to retract at a constant rate, which allowed the tank pressure to expand the gold cell with a (headspace) volume of H_2 roughly equivalent to the water volume received in the pump. Sufficient H_2 was added to yield an estimated concentration of 10–20 mmolal, which is on the high end of values measured in deep sea hydrothermal fluids (Charlou et al., 2002; Gallant and Von Damm, 2006; Schmidt et al., 2007; Seyfried et al., 2011, 2015; McDermott et al., 2015). With the gold cell then effectively charged (Ti valve now closed), the furnace was inverted (the sampling tube/valve now facing the floor) in order to distance the H_2 bubble(s) from the sampling assembly before raising the system pressure. This minimizes the amount of gas that might be compressed in and around the sampling line, which would otherwise hinder the rate of dissolution, and also mitigates the risk of the first fluid sample being inhomogeneous. The system was pressurized to 200 bars to speed H_2 dissolution, and the first sample was acquired after 4.5 hrs. Thereafter the *P* was lowered and maintained at 70 bars for all *T* conditions, which is (arbitrarily) ~3× higher than saturation for a solution of 20 mmolal H_2. Due to the relatively large *T* dependence of D/H fractionation between H_2 and H_2O (Fig. 1), we were able to retrieve rate constants for multiple temperatures (97, 54 and 22 °C) within a single experiment (see below). Temperatures reported herein refer to a steel-sheathed type K thermocouple (chromel-alumel) in direct contact with the confining fluid surrounding the gold cell. The temperature gradient in the system was assessed by rocking the (tubular) furnace from horizontal through vertical orientations, which redistributes heat flow relative to the static (horizontal) position maintained over the duration of the experiment. During this process, *T* varied by less than 2 °C, which is comparable to the uncertainty of the thermocouple. For the final leg of the experiment, the furnace *T* controls were shut off, and the system cooled to that of ambient in the laboratory. The laboratory is climate controlled year round, and the system read between 21 and 23 °C for the duration.

Gas-tight samples were acquired over the course of the experiment for quantitative analysis of dissolved H_2 and δD_{H2}. Samples for dissolved H_2 were taken into plastic syringes with a PTFE stopcock for immediate analysis by gas chromatography. This measurement was performed periodically to assure the H_2 concentration in the gold cell was not changing with time. A steady-state concentration of 18 mmolal was observed. Samples for δD_{H2} were expressed directly from the reaction cell into sterile 60 ml pyrex vials, sealed with crimped butyl rubber stoppers. The sampling assembly and procedure was as follows. Two fine-gauged luer-lock needles were inserted through the stopper of the pyrex vial. Needle (1) was connected to the Ti sampling valve using a 3-way PTFE stopcock (one extra "bleed" port was available). Needle (2) was connected to a tank of grade 6 He gas. In this way, both the vial and sampling assembly were thoroughly purged with He: in through needle (2) and out the bleed port of the stopcock, which had a length of tubing that terminated under water to observe bubbling and prevent back flush. With He still flowing, needle (2) was removed from the vial, and when bubbling ceased, communication from the stopcock to the vial was closed. An empty syringe was placed in the bleed port, and the Ti sampling valve was carefully opened until the syringe plunger slowly began moving. Once 1–2 mls of water had accumulated in the syringe, communication was switched from the bleed port to the vial. The bleed process served to discard the fluid fraction from the sampling line that was not at full experimental *T*. Once 2–3 mls of water (plus exsolved H_2) had accumulated in the vial, the sampling valve was closed and the vial stored for later analysis (see below). We note this sampling process naturally imparted a slight over-pressure in the vial, which allowed us to easily acquire multiple subsamples of the gas headspace.

2.2. Analytical methods for the D/H (isotope) ratios of H_2 and H_2O

The isotopic composition of H_2 was analyzed at the Center for Isotope Geochemistry (Lawrence Berkeley National Laboratory) using a Thermo Scientific GC Trace Gas Ultra system connected to a Thermo Scientific Delta V Plus Mass Spectrometer (IRMS). A volumetrically calibrated sample loop attached to a 6-port valve system was flushed with sample gas, and the gas then injected onto the GC column. H_2 was separated on an HP-molesieve fused silica capillary column (30 m × 0.320 mm) prior to passing into the IRMS. Reproducibility of these analyses is ±5‰ (2σ), as determined by repeated analyses of 3 calibrated gas standards ($\delta D_{H2(VSMOW)} = -762$, −364 and −124‰). Linearity of the IRMS is also observed within the uncertainty noted above. Although the δD_{H2} values measured in our experiments fall outside the range calibrated on our instrument, there is little reason to expect this is problematic because they amount to a modest (<2.5×) increase in the D/H ratio relative to natural abundance. Furthermore, previous studies have demonstrated excellent linearity for δD_{H2} by IRMS over several orders of magni-

tude (e.g., Hilkert et al., 1999; Morrison et al., 2001; Tobias et al., 1995). Experimental samples were also re-analyzed at various (later) time intervals over the course of the study to make sure there was no significant change in δD_{H2} values during storage (at ambient T) between sampling and analysis. The replicate analytical results differ by no more the 16‰ (average 8‰), indicating that once the H_2 was degassed and diluted in the sample vial, the isotopic composition was effectively stable over storage times employed (Table 1).

A deuterium-enriched water was used in the experiment to ensure the system was initially far from isotopic equilibrium, and to facilitate large changes in δD_{H2} that could be well resolved analytically with reaction progress. The starting water was a mixture of 0.51 g of 99.9% D_2O and 554.92 g of de-ionized water ($\delta D_{H2O} = +86‰$), which produced water with a δD_{H2O} of ~+5200‰. Despite the large shifts in δD_{H2} in the experiments, the mass balance of water in the system was sufficiently high that comcomitant changes in δD_{H2O} were calculated to be negligible (<0.5‰). The actual δD of the water was analyzed using a Los Gatos Research liquid water analyzer (LGR). This required serially diluting the solution with additional de-ionized water to within the calibrated linear range of the LGR (≤+836‰). Within uncertainty, no difference in δD_{H2O} was observed between the unreacted starting water and water recovered from the Au experimental cell upon conclusion of the experiment. Based on these measurements, we calculated a δD_{H2O} value of +5220 ± 50‰ (2σ) for the experimental water. This uncertainty is not critical when determining the kinetic rate constants from our experiments because these are based only on relative changes in δD_{H2} (see Section 3.1). However, this does introduce a relatively large error in calculations of the equilibrium isotope fractionation factors ($\alpha_{H2O\text{-}H2(eq)}$) at the 3 temperatures used for these experiments (see Section 4.2).

3. RESULTS

The raw experimental data are shown in Table 1 and Fig. 3. At the three temperatures studied, near equilibrium conditions were ultimately achieved, indicated by an approach to steady-state δD_{H2} with time (Fig. 3). Observing the time series changes in δD_{H2}, isotopic equilibrium was reached on timescales of ~250 hrs at 97 °C, ~1,500 hrs at 54 °C, and >12,000 hrs at 22 °C. This corresponds to half lives for isotope exchange of about 2 days, 2 weeks, and 3 months at 97, 54 and 22 °C, respectively. The data also demonstrate that D–H isotope exchange between H_2O and H_2 is reversible. As discussed in more detail below, deriving appropriate rate constants for such reversible reactions requires defining the equilibrium value (e.g., Lasaga, 1998). In many instances, chemical reactions subject to kinetic studies do not equilibrate on laboratory timescales, which necessitates constraining expected equilibrium using empirical or theoretical relationships. For example, Fig. 3 compares our experimental results with equilibrium values of δD_{H2} (or $\delta D_{H2(eq)}$) calculated using the measured δD_{H2O} ($\approx\delta D_{H2O(eq)}$, +5220‰) and equations for $\alpha_{H2O\text{-}H2(eq)}$ after both Bardo and Wolfsberg (1976) and

Table 1
Experimental change in δD_{H2} (VSMOW) of dissolved H_2 with time (t).

t (hrs)[a]	δD_{H2} (‰)	Δt (days)[b]	t (hrs)	δD_{H2} (‰)	Δt (days)
97 °C and 70 bars			*54 °C and 70 bars*		
0.0	−107		0.0	1383	18
4.5	35		0.0	1386	181
22.8	512	6	3.7	1383	
22.8	514	611	14.7	1371	
47.8	853		27.5	1360	17
77.1	1096		27.5	1363	180
95.6	1225	3	47.1	1344	16
95.6	1215	17	47.1	1357	179
143.6	1337	1	114.6	1298	
143.6	1323	15	163.6	1261	11
192.6	1365		163.6	1254	174
244.6	1377		209.0	1237	
335.6	1390	7	261.5	1209	
335.6	1384	598	360.7	1153	166
381.8	1383	5	360.7	1140	555
381.8	1400	44	474.4	1114	
1004.8	1390	18	578.1	1090	
1004.8	1388	181	740.6	1050	
22 °C and 70 bars			835.7	1045	
0.0	990		1078.0	1015	
6864.0	668		1244.4	1013	
9432.0	648		1580.3	998	
11376.0	639		2061.0	995	

[a] Time normalized for each temperature.
[b] Time between sampling and analysis, demonstrates no meaningful change in δD_{H2} during sample storage.

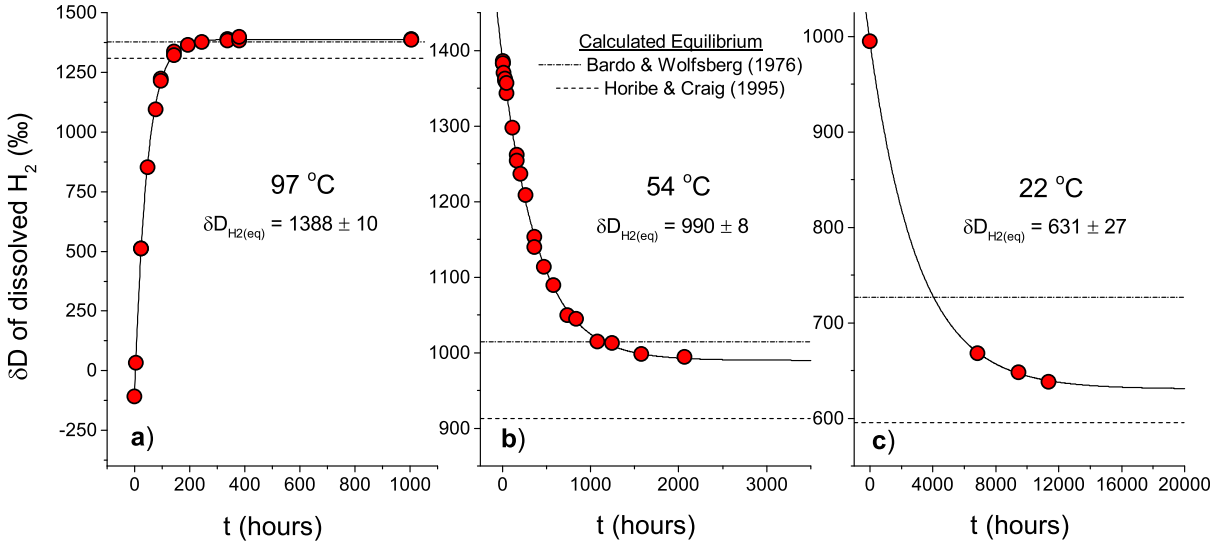

Fig. 3. Change in D/H composition of dissolved H_2 (δD_{H2}) with time (t) at (a) 97 °C, (b) 54 °C, and (c) 22 °C. Equilibrium was closely approached for all three temperatures (note t is normalized to zero in each panel relative to total duration of experiment (Table 1). Experimental data were fit with an exponential function of form $y = y_0 + Ae^{-x/B}$, where asymptote is y_0, or expected equilibrium value ($\delta D_{H2(eq)}$, reported uncertainties are 95% confidence intervals). These values were used to derive respective rate constants (Fig. 4), and to compare results with predicted equilibrium values (Fig. 7). Values of $\delta D_{H2(eq)}$ calculated using two different T vs. $\alpha_{H2O\text{-}H2(eq)}$ relationships (see also Section 4.2, Fig. 7) and the experimental δD_{H2O} value (+5220‰) shown for comparison (dashed lines).

Horibe and Craig (1995). Despite general agreement, neither of these relationships best reflect the approach to equilibrium exhibited in the experiments at all three temperatures. Therefore, to extract accurate and internally consistent rate constants, values of $\delta D_{H2(eq)}$ were extrapolated by fitting the experimental data from each T with an exponential function (Fig. 3), rather than depending on theoretically calculated values. Using these data, we describe in the following section the derivation of rate constants for D–H exchange between liquid H_2O and dissolved H_2 (or $H_{2(aq)}$).

3.1. Derivation of rate constants for D–H isotope exchange and their temperature dependence

In our experimental system, D_2O and $D_{2(aq)}$ species should be negligible because of the small abundance of D relative to H, so the reversible reaction under consideration may be represented as the exchange of one D between dissolved hydrogen and water:

$$H_2 + HDO \leftrightarrow HD + H_2O \quad (2)$$

Assuming first-order rate dependence for all species (e.g., Cole and Chakraborty, 2001) we can write the following differential equation in which reaction progress is traced by the change in the concentration of HD with time (t);

$$d[HD]/dt = k'[H_2][HDO] - k[HD][H_2O] \quad (3)$$

and k' and k represent forward and reverse rate constants, respectively (Criss et al., 1987; Criss, 1999; Cole and Chakraborty, 2001). If the concentrations are expressed in units of moles per liter (mol/L), the k values have units of, for example, [L/mol]/hr. Isotopic equilibrium is attained when $d[HD]/dt = 0$, and this condition can therefore be described with the following expression:

$$\frac{k'}{k} = \frac{[HD_{(eq)}][H_2O_{(eq)}]}{[H_{2(eq)}][HDO_{(eq)}]} \quad (4)$$

where ratio k'/k is the equilibrium D/H fractionation factor (α_{eq}) for H_2 in equilibrium with H_2O. For reaction progress at any time between $t = 0$ and equilibrium, the mass balance in our experiment was designed such that changes in all species other than [HD] were sufficiently negligible to allow the simplifying assumption that their concentrations remain equal to the starting values, which means they can also be represented as the equilibrium values. Therefore Eq. (3) may be written as;

$$d[HD_{(t)}]/dt = k'[H_{2(eq)}][HDO_{(eq)}] - k[HD_{(t)}][H_2O_{(eq)}] \quad (5)$$

and subsequently integrated to yield:

$$[HD_{(t)}] = \frac{k'[H_{2(eq)}][HDO_{(eq)}]}{k[H_2O_{(eq)}]} + Ce^{-k[H_2O_{(eq)}]t} \quad (6)$$

where C is the integration constant. The right side of Eq. (4) may be substituted for the k'/k term in Eq. (6), which simplifies to;

$$[HD_{(t)}] = [HD_{(eq)}] + Ce^{-k[H_2O_{(eq)}]t} \quad (7)$$

At $t = 0$, $[HD_{(t)}] = [HD_{(i)}]$, the initial concentration of HD, and therefore $C = [HD_{(i)}] - [HD_{(eq)}]$. Further defining $k[H_2O_{(eq)}] = k_1$, the effective rate constant, we arrive at the expression:

$$\frac{[HD_{(t)}] - [HD_{(eq)}]}{[HD_{(i)}] - [HD_{(eq)}]} = e^{-k_1 t} \quad (8)$$

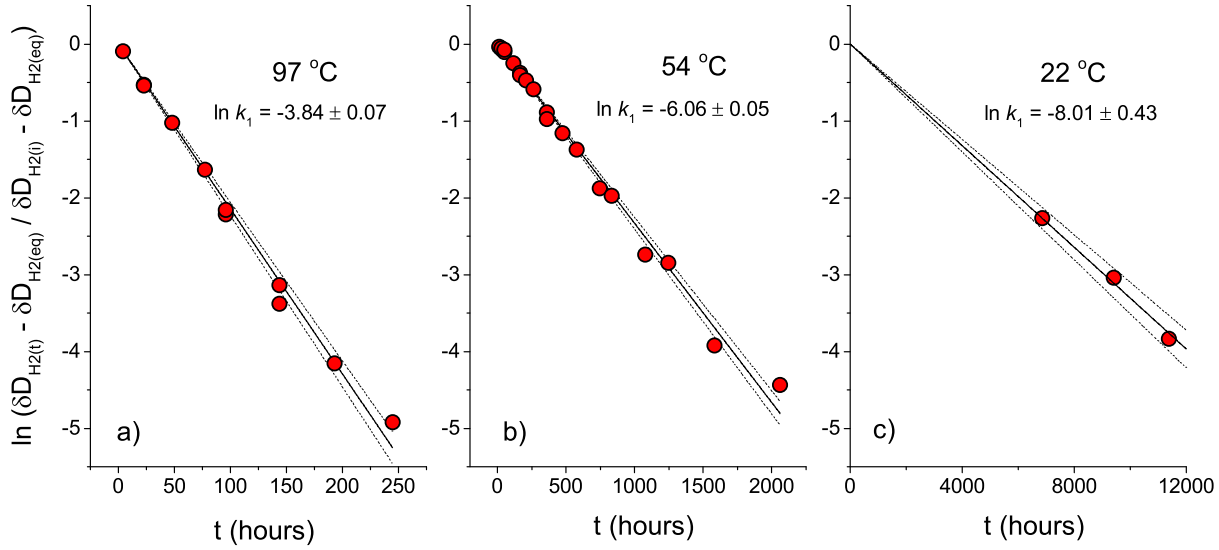

Fig. 4. Experimental data cast in form of fractional approach to equilibrium with time (t) at (a) 97 °C, (b) 54 °C, and (c) 22 °C (see Eqs. (8), (9)). Slope of linear regressions yield rate constants (k_1, in hr^{-1}), where dashed lines and reported uncertainty in k_1 both represent 95% confidence. All three regressions were forced to intercept origin, though data at 97 and 54 °C did so naturally within uncertainty. Data for t > 245 hrs in the 97 °C experiment are not included in the regression because the measured δD_{H2} values are at or beyond the extrapolated equilibrium value within analytical reproducibility (cf Table 1, Fig. 3).

This represents a pseudo-first-order expression, and the left side of Eq. (8) equates to the fractional approach to equilibrium, often denoted as the quantity 1 − F (i.e. F = 1 at equilibrium), and may be equivalently cast in terms of isotope ratios (e.g., D/H) or delta (δ) values (Criss et al., 1987; Criss, 1999; Cole and Chakraborty, 2001). For convenience, we use the measured δD_{H2} values in the following expression to treat our experimental data:

$$\ln \frac{\delta D_{H2(t)} - \delta D_{H2(eq)}}{\delta D_{H2(i)} - \delta D_{H2(eq)}} = -k_1 t \quad (9)$$

If the assumption of first-order behavior is appropriate, the left side of Eq. (9), plotted versus time, should be linear, with slope = $-k_1$, and intercept at the origin. Regressions of the isotopic data and the derived rate constants (k_1) using Eq. (9) are shown in Fig. 4; and an associated Arrhenius plot displays an excellent correlation with T, yielding an activation energy (E_a) of 52 kJ/mol (Fig. 5).

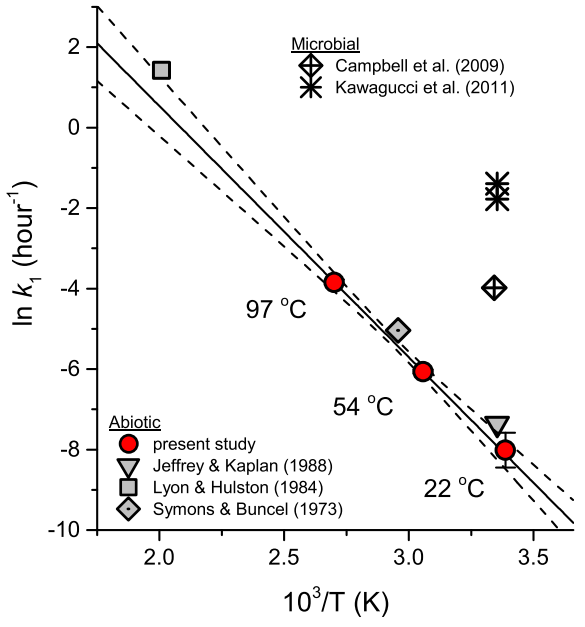

Fig. 5. Arrhenius plot depicting T dependence of rate constants (k_1) derived in Fig. 4. A weighted linear regression of new experimental data yields: ln k_1 = 13.0 (±0.2) − 6238 (±61)/T (2σ uncertainty) with R^2 = 0.9998. Dashed lines represent 95% confidence interval. Slope gives activation energy (E_a) of 51.9 kJ/mol. Literature data shown for comparison were not included in regression (see Section 4).

4. DISCUSSION

Previously published data that is directly comparable to our liquid-phase D–H exchange rates are scarce. Lyon and Hulston (1984) note a half-life of ~10 mins at 225 °C, and Jeffrey and Kaplan (1988) report a shift in δD_{H2} from −195 to −672‰ (δD_{H2O} = −92‰) after 4 months at ~25 °C. These observations, although not fully documented in the papers, are nonetheless consistent with our results (Fig. 5). Our experiment was conducted at sub-neutral pH (~5.6 at 22 °C), and we note several other laboratory studies indicate the rate of isotope exchange with H_2 is catalyzed by high concentrations of hydroxide ion, whereas increasing acidity seems to have little effect (Wilmarth et al., 1953; Miller and Rittenberg, 1958; Flournoy and Wilmarth, 1961). The extent to which rates reported in these previous studies are quantitatively comparable to ours is uncertain because data are typically not tabulated, and they were mostly derived from systems where steam was

coexisting with highly basic solutions (≫0.1 molal [OH^-]). These other studies were concerned with the mechanism of hydroxide catalysis to the extent that a *T*-independent "background rate" for reaction with solvent water was subtracted for solutions where [OH^-] < 1 molal (Flournoy and Wilmarth, 1961). While hydroxide catalysis appears considerable, the relative effect within the range of [OH^-] observed in natural solutions may be less significant. For example, in a 0.011 molal hydroxide solution at 65 °C, Symons and Buncel (1973) calculate a k_1 value 1.5× larger than we observe (Fig. 5). This is a modest enhancement of the kinetics for a solution that amounts to a pH (25 °C) of ~12, which is on the high end of values reported from natural alkaline springs (e.g., Neal and Stanger, 1983; Suda et al., 2014; Etiope et al., 2017). Considering the heterogeneity of natural aqueous solutions, there is nonetheless potential for other dissolved components to affect rates of isotope equilibration between H_2 and H_2O. In addition, microbial metabolism can significantly speed progress towards equilibrium (Romanek et al., 2003; Valentine et al., 2004; Vignais and Billoud, 2007; Campbell et al., 2009; Kawagucci et al., 2011, 2014; Okumura et al., 2016).

Given currently available constraints, the expression for k_1 shown in Fig. 5 appears acceptable for generally representing uncatalyzed rates of D–H exchange between $H_{2(aq)}$ and liquid H_2O. However, the experiments of Lecluse and Robert (1994) suggest exchange rates (k_1) in the gas phase are slower by several orders of magnitude. In the next section, we therefore compare our new results to the gas-phase data of Lecluse and Robert (1994), with the aim of developing a universal rate expression that accounts for how phase changes impact the isotope exchange kinetics. Isotope fractionation between gas/vapor and liquid phases also plays a role in accounting for the variability in predicted equilibrium D/H fractionation ($\alpha_{H2O\text{-}H2(eq)}$), exemplified in Fig. 3. The implications of this are discussed in Section 4.2, where we use the best available data to derive updated representations for the temperature dependence of $\alpha_{H2O\text{-}H2(eq)}$. In subsequent Sections 4.3–4.6 we use the new kinetic and equilibrium relationships obtained in Sections 4.1 and 4.2, respectively, to build kinetic models that can account for non-equilibrium D/H fractionation where observed in natural geologic systems.

4.1. A general expression for D–H exchange rates in both gaseous and liquid systems based on phase density

The simplicity of Eq. (9) suggests it may be possible to extend rates of D/H equilibration in liquid water to systems that are dominated by gas phases. To evaluate this we compare our experimental results to those of Lecluse and Robert (1994), who derived rate data from individual batch reactions between H_2 and D_2O gas, carried out in a glass tube apparatus. These gas phase reactions were performed with and without the presence of potential natural catalysts, the objective being to understand isotopic evolution in the solar nebula. They report the initial partial pressures of each gas at ambient *T* (total *P* averaged ~0.08 atm), and the change in D/H ratio of the H_2 gas after reaction for a given time at temperatures up to 400 °C.

Lecluse and Robert (1994) concluded that the catalysts they employed had no meaningful effect on rates of D–H exchange, and treated all of their data together. However, due to what we perceive as inconsistencies, we eliminate from consideration their results from experiments conducted with either activated charcoal or montmorillonite (clay). For example, Lecluse and Robert (1994) note that rates obtained from experiments with charcoal appear systematically faster, despite the difference being statistically insignificant. In addition, many of the experiments conducted with charcoal and clay utilized substrate the authors had pre-enriched with D_2O, and in several of these cases they report D_2O partial pressures in excess of steam-saturation pressure at the applicable *T*, with the derivation of these values being unclear. We also neglect data for $T < 100$ °C because the rates depicted graphically in Lecluse and Robert (1994) are much lower than those that can be calculated using their tabulated data. More specifically, the average rates calculated for 65 °C (2 experiments) and 25 °C (11 experiments) are both higher than that at 100 °C (11 experiments), in which case the authors note (for an unspecified number of experiments) that, "when no exchange was detected, rate constants are not reported in the tables but were taken into account in the mean values plotted in [figures]". The remainder of the data we evaluate below consist of 40 experiments conducted at temperatures between 100 and 400 °C.

One important difference between our experiments and those of Lecluse and Robert (1994) is that their starting reactant was D_2O, a species we assumed to be of negligible concentration in our experiments. The exchange reaction they investigated was therefore:

$$H_2 + D_2O \leftrightarrow HD + HDO \tag{10}$$

and the reaction rate is then written as:

$$d[HD]/dt = k'[H_2][D_2O] - k[HD][HDO] \tag{11}$$

Lecluse and Robert (1994) ultimately derived an equation analogous to Eq. (9) to describe their experiments, expressed in the following form:

$$\ln\frac{2[D/H]_{H2(t)} - X_{D2O}}{2[D/H]_{H2(i)} - X_{D2O}} = -k_1 t \tag{12}$$

where

$$X_{D2O} = \frac{[D_2O_{(i)}]}{[D_2O_{(i)}] + [H_{2(i)}]} \tag{13}$$

and

$$k_1 = \frac{k'([D_2O_{(i)}] + [H_{2(i)}])}{\alpha_{H2O-H2(eq)}} \tag{14}$$

Equations (12)–(14) were used to extract k_1 and k values using the raw data of Lecluse and Robert (1994), recognizing that $k' = k/\alpha_{H2O\text{-}H2(eq)}$. Although these authors cast their rates in terms of gas partial pressures, we instead used concentration units of mol/L, because this simultaneously accounts for system density, and is ultimately more conducive to comparing rates observed in the gas phase with those in liquid H_2O. In this case the units of k are then [L/mol]/hr. Recalling our derivation of k_1 in condensed

H_2O (Section 3.1, Eqs. (7), (8)), we defined k_1 (hr^{-1}) = k [H_2O]. We therefore calculated k values using the k_1 data given in Fig. 4 and the density of pure water at each T and P (~55 mol/L). The results show excellent agreement between our experiments and those of Lecluse and Robert (1994) for the T dependence of the rate constants k (Fig. 6a). A weighted regression of the combined datasets yields the following relationship;

$$\ln k = 9.186 - 6298/T \quad (15)$$

where k is in units of [L/mol]/hr, and T is absolute temperature (K).

In general, for any $H_2O + H_2$ system, regardless of phase, we infer that the effective first-order constant (k_1) that will describe the rate of approach to isotopic equilibrium is:

$$k_1 = k([H_2O] + [H_2]) \quad (16)$$

where [H_2O] and [H_2] are the concentrations of each species (including isotopologues) in mol/L, which will be a function of T, P, and the full chemical composition of the system. Under many circumstances, we may consider $k_1 \approx k$[H_2O] to adequately represent the rate constant because H_2O is usually the predominant component. This then yields a simplified full expression for k_1;

$$k_1 = 9764.61[H_2O]e^{-6298/T} \quad (17)$$

where [H_2O] may be constrained as the density of water at the T and P of interest (ρ_W, in mol/L), and k_1 has units of hr^{-1}. The overall T dependence yields an E_a of 52.4 ± 1.3 kJ/mol (95% CI), which is (expectedly) within the uncertainty of that derived in Fig. 5 because the lower uncertainty of our data carried greater weight in the regression (Fig. 6a). However, an independent extrapolation of the k_1 values derived from Lecluse and Robert (1994) gives a similar value of 48 ± 14 kJ/mol, which indicates the same reaction mechanism in both condensed water and gas scenarios, suggesting the isotope exchange rate may be largely a function of molecular collision frequency. The broader use of our simple density-based relationships therefore seems reasonable until more data become available.

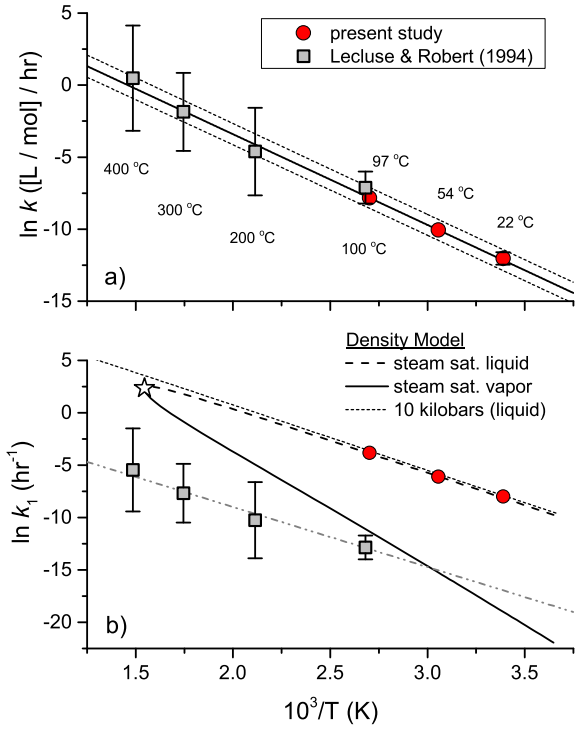

Fig. 6. Arrhenius style plots showing density-based rate model for D–H exchange between H_2 and H_2O. Panel (a) shows data from present study, and those recast from Lecluse and Robert (1994), where both datasets are "normalized" to system density of 1 mol/L (see Section 4.1). Historical data points represent average of 11 (ln $k = -7.12 \pm 1.11$), 15 (ln $k = -4.61 \pm 3.04$), 10 (ln $k = -1.86 \pm 2.71$), and 4 (ln $k = 0.48 \pm 3.65$) individual batch experiments conducted at 100, 200, 300 and 400 °C, respectively, and error bars are 2σ. A weighted regression of combined data sets gives: ln k (in [L/mol]/hr) = 9.186 (±0.18) − 6297 (± 63)/T (2σ uncertainty), where dashed lines represent 95% prediction limit, and associated $E_a = 52.4 \pm 1.3$ kJ/mol (95% CI). Panel (b) presents effective first order k_1 values (hr^{-1}) for both experimental datasets. Stand-alone regression of k_1 values from Lecluse and Robert (1994) gives $E_a = 48 \pm 14$ kJ/mol (95% CI), consistent with other regressions (above and Fig. 5) despite higher uncertainty. Experimental data are compared with calculated k_1 values (using Eq. (17)) along vapor and liquid curves of pure H_2O (star is critical point), and also a high pressure isobar (10,000 bars). The latter demonstrates how incompressibility of liquid water should result in less variability in isotope exchange rate relative to vapor phases.

In order to provide an example of the predicted effect of density on the isotope exchange rate, we use Eq. (17) to calculate and compare k_1 values along the vapor and liquid branches of the H_2O steam saturation curve (Fig. 6b). For pure H_2O, at any given T along this curve (between 0 °C, the freezing point, and 374 °C, the critical point), system pressure is fixed by the coexistence of liquid H_2O and saturated H_2O vapor. Although the fugacity of H_2O in both the liquid and vapor are equivalent (at any fixed T), the difference in the density of H_2O between the coexisting phases can be substantial. Fig. 6b implies that the effective k_1 in a closed (and isothermal) system, where saturated H_2O vapor exists, should lie somewhere between the two end-member k_1 values calculated for the vapor and liquid phases, depending roughly on the volume fraction of each phase. However, the natural occurrence of immiscible phases in most geological settings is the result of open system conditions, where solutions experience changes in temperature and/or pressure; and differences in the density of these phases, once developed, also promotes their segregation.

4.2. Updated representations for the temperature dependence of equilibrium isotope fractionation in the H_2–H_2O system

The equilibrium values of δD_{H2} derived by extrapolation of curves fit to our experimental data (Fig. 3) provide an independent comparison of our results with the predicted T-dependent equilibrium fractionation between H_2O and H_2 ($\alpha_{H2O\text{-}H2(eq)}$). The new data compare favorably, falling between representative curves for gaseous H_2 in equilibrium with H_2O liquid (denoted $\alpha_{H2O(L)\text{–}H2(g)}$) and H_2O vapor (denoted $\alpha_{H2O(v)\text{–}H2(g)}$, Fig. 7), where the $\alpha_{H2O(v)\text{–}H2(g)}$ and $\alpha_{H2O(L)\text{–}H2(g)}$ curves differ by the vapor–liquid isotope

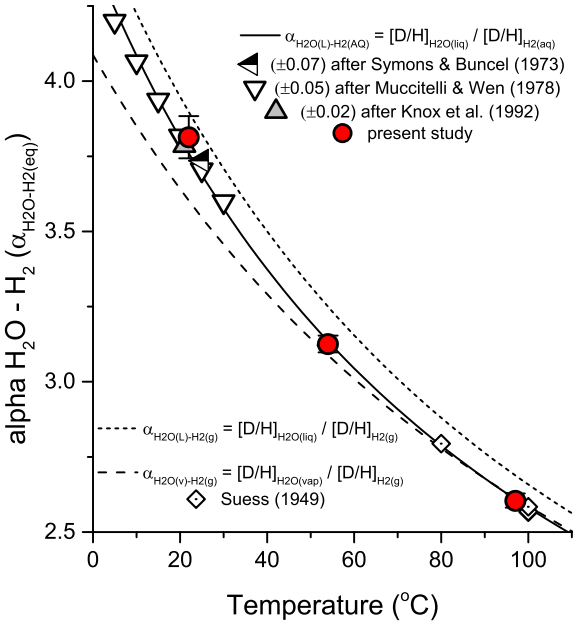

Fig. 7. Equilibrium isotope (D/H) fractionation between H_2O and H_2 ($\alpha_{H2O\text{-}H2(eq)}$) as a function of T. Experimental $\alpha_{H2O\text{-}H2(eq)}$ values are calculated as $(\delta D_{H2O(eq)} + 10^3)/(\delta D_{H2(eq)} + 10^3)$ using data from Fig. 3 and $\delta D_{H2O(eq)} = +5220 \pm 50‰$ (2σ). This yields 2.605 ± 0.024 (97 °C), 3.126 ± 0.028 (54 °C), and 3.814 ± 0.070 (22 °C). Compared are equilibrium curves for gaseous H_2 coexisting with liquid H_2O ($\alpha_{H2O(L)–H2(g)}$) and H_2O vapor ($\alpha_{H2O(v)–H2(g)}$). New data was used in defining $\alpha_{H2O(liq)–H2(aq)}$ or $\alpha_{H2O(L)–H2(AQ)}$ (solid line), along with values calculated using $\alpha_{H2O(L)–H2(g)}$ and corresponding $\alpha_{H2(aq)–H2(g)}$ values taken from Knox et al. (1992), Muccitelli and Wen (1978) and Symons and Buncel (1973). Estimated uncertainties for these data are given in legend for clarity. Note $\alpha_{H2O(v)–H2(g)}$ and $\alpha_{H2O(L)–H2(g)}$ are comparable to relationship given by Bardo and Wolfsberg (1976), and Eq. (8) of Horibe and Craig (1995), respectively, in T range shown. The three $\alpha_{H2O\text{-}H2(eq)}$ curves may be calculated using coefficients given in Table 2. See Section 4.2 and Supplementary Information for derivation.

(D/H) fractionation factor of H_2O (Horita and Wesolowski, 1994; Horibe and Craig, 1995). The $\alpha_{H2O(L)–H2(g)}$ curve has previously been used to describe equilibrium for H_2 dissolved in liquid H_2O, but this would only be correct if there were no isotope fractionation between gaseous and dissolved H_2 (or $H_{2(g)}$ and $H_{2(aq)}$, respectively). However, Knox et al. (1992) report a $H_{2(aq)}$–$H_{2(g)}$ isotope fractionation factor of 1.037 at 21 °C. When this is factored with the $\alpha_{H2O(L)–H2(g)}$ relationship, it results in a fractionation factor of 3.786 (grey triangle, 21 °C, Fig. 7), which is within the uncertainty of what we report for liquid H_2O and $H_{2(aq)}$.

The $\alpha_{H2O(v)–H2(g)}$ and $\alpha_{H2O(L)–H2(g)}$ curves in Fig. 7 ultimately converge with increasing T along the vapor-liquid envelope of water. Beyond this region, experimental and theoretical calculations still largely concern coexistence of H_2 with H_2O vapor, which may not best reflect isotopic fractionation in higher density crustal fluids (Foustoukos and Mysen, 2012). Nonetheless, potential differences are likely to be small, especially for purposes of geothermometry at high temperatures, where equilibrium α values converge and approach unity (Criss, 1999). For example, the data of Fu et al. (2007) yield a reproducible $\alpha_{H2O\text{-}H2}$ of 1.47 at 400 °C and 500 bars, which falls within the range of $\alpha_{H2O\text{-}H2(eq)}$ values predicted by currently established ($\alpha_{H2O(v)–H2(g)}$) correlations (Suess, 1949; Bardo and Wolfsberg, 1976; Richet et al., 1977). Equilibrium isotope fractionation factors become more uncertain with decreasing T, considering the exponential increase in $\alpha_{H2O\text{-}H2(eq)}$, and a paucity of experimental data for $T < 100$ °C (even in the gaseous system).

Using the limited low-T data for $\alpha_{H2O\text{-}H2(eq)}$, including those herein, we have produced an equilibrium curve for isotope fractionation between $H_2O_{(liq)}$ and $H_{2(aq)}$, which we refer to as $\alpha_{H2O(L)–H2(AQ)}$ (Fig. 7, Supplementary Information). This was done by first regressing a new $\alpha_{H2O(v)–H2(g)}$ curve, combining experimental and theoretical data where good agreement is observed (Suess, 1949; Bardo and Wolfsberg, 1976; Fu et al., 2007). Similar to Horibe and Craig (1995), we then derived a new relationship for $\alpha_{H2O(L)–H2(g)}$ using the vapor–liquid (D/H) fractionation factors of H_2O given by Horita and Wesolowski (1994). These $\alpha_{H2O(v)–H2(g)}$ and $\alpha_{H2O(L)–H2(g)}$ curves provided a basis for establishing a reasonable and internally consistent representation of $\alpha_{H2O(L)–H2(AQ)}$. The $\alpha_{H2O(v)–H2(g)}$ and $\alpha_{H2O(L)–H2(g)}$ curves coincide for $T > \sim 220$ °C, and the data of Fu et al. (2007), obtained at supercritical T and P, support the assumption that $\alpha_{H2O(L)–H2(AQ)} = \alpha_{H2O(v)–H2(g)}$ at these conditions. The new $\alpha_{H2O(L)–H2(AQ)}$ regression therefore included calculated values of $\alpha_{H2O(v)–H2(g)}$ for this (higher) T range. Data constraining the lower T range of the regression are shown in Fig. 7, which, in addition to our results, includes values calculated using $\alpha_{H2O(L)–H2(g)}$ and previously published $H_{2(aq)}$–$H_{2(g)}$ isotope fractionation factors, as exemplified by the Knox et al. (1992) datum noted above (see Supplementary Information for further details). Table 2 provides new polynomial coefficients for calculating $\alpha_{H2O\text{-}H2(eq)}$ in the H_2–H_2O system. These relationships indicate $\alpha_{H2O(v)–H2(g)} \approx \alpha_{H2O(L)–H2(AQ)}$ for $T > 110$ °C, and the 95% prediction limits are $\alpha_{H2O(v)–H2(g)} \pm 0.018$ and $\alpha_{H2O(L)–H2(AQ)} \pm 0.025$, although these uncertainties increase for $T < 15$ °C (see Fig. S4).

When comparing field data (α_{OBS}) to equilibrium fractionation there is generally some uncertainty about which $\alpha_{H2O\text{-}H2(eq)}$ applies (Fig. 7), because it will depend on the nature of the sample and how it was acquired. In open (natural) systems, the low aqueous solubility of H_2 may result in exsolution prior to or during sampling such that whether

Table 2
Polynomial coefficients for equilibrium D/H fractionation[a,b] in the water-hydrogen system: $\alpha_{H2O\text{-}H2(eq)} = A + B/T^2 + C/T^4 + D/T^6$.

$\alpha_{H2O\text{-}H2(eq)}$	$H_2O_{(vap)}/H_{2(g)}$ ($\alpha_{H2O(v)–H2(g)}$)	$H_2O_{(liq)}/H_{2(aq)}$ ($\alpha_{H2O(L)–H2(AQ)}$)	$H_2O_{(liq)}/H_{2(g)}$ ($\alpha_{H2O(L)–H2(g)}$)[c]
A	0.9997	1.00138	1.01847
B	218,170	219,788	200,833
C	−2.056E+08	−2.926E+09	2.899E+09
D	8.315E+13	4.108E+14	1.289E+14

[a] Input is absolute T (K).
[b] Regression statistics given in Supplementary Information.
[c] Assumes H_2O liquid and vapor coexist, $0 \le T < 374$ °C.

to reference $\alpha_{H2O(L)–H2(AQ)}$ or $\alpha_{H2O(L)–H2(g)}$ requires considering mass balance. For example, if kinetic isotope effects are minimal, it might be reasonable to expect that δD_{H2} measured in free gas that has exsolved from continental spring waters should be referenced to $\alpha_{H2O(L)–H2(g)}$ ($H_2O_{(liq)}$–$H_{2(g)}$, given δD_{H2O} is usually measured in the liquid). This assumes vapor–liquid isotopic equilibrium was achieved during degassing, whether or not the previously dissolved H_2 was in equilibrium with the H_2O. However, this assumption is generally unnecessary because gas/liquid distribution coefficients (K_d) for H_2 exceed $7 * 10^4$ for $T < 100$ °C (Fernandez-Prini et al., 2003), making it difficult to shift the δD_{H2} of exsolved gas relative to the δD_{H2} of the bulk system unless D–H exchange with H_2O in the gas (or vapor) can occur. Sufficient exchange is unlikely due to the sluggish kinetics in a gas/vapor phase even at 100 °C (e.g., $1/k_1 \approx 7$ yrs vs. ~2 days in the liquid, Fig. 6b). Therefore $\alpha_{H2O(L)–H2(AQ)}$ ($H_2O_{(liq)}$–$H_{2(aq)}$) is usually the best equilibrium reference whenever the sampled water phase is a liquid. Ultimately, the apparent T of samples calculated using $\alpha_{H2O(L)–H2(AQ)}$ are as much as ~8 °C lower than those derived using $\alpha_{H2O(L)–H2(g)}$, which is a modest uncertainty. However, the distinction has greater impact on results of kinetic models, especially at lower T, because time to equilibration is proportional to the degree of isotopic disequilibrium (Eq. (9)).

4.3. Application of kinetic models to D/H isotope fractionation observed in natural geologic systems

When T at the point of sampling is known, our kinetic data allow us to use the δD values of H_2 and H_2O measured in natural fluids (Fig. 1) to infer aspects of hydrology such as fluid transit times in the crust and their average flow velocity, depending on the availability of additional constraints. Here we focus mostly on interpreting data from hydrothermal and volcanic systems. We develop simple kinetic models of D–H exchange that simulate effects of cooling as fluids/gases flow up through the crust; away from a high-T (magmatic) heat source, where H_2 and H_2O are likely to be in isotopic equilibrium, and towards the surface, where samples are obtained. The models use the first-order rate (Eq. 9), and the T-ρ_W-dependent expression for k_1 (Eq. (17)) to calculate how δD_{H2} evolves as a function of a specified cooling rate and the initial T of H_2–H_2O isotopic equilibrium. For example, the kinetic fractionation trends shown in Figs. 8–10 (see Sections 4.4 and 4.5 below) were derived by calculating the change in δD_{H2} with incremental (step-wise) decreases in T of 0.5 °C, where k_1 is a function of T and an assumed P (i.e. T and P yield density), and t (hrs) across each step is a function of the imposed conductive cooling rate (°C/hr). For the geologic scenarios subsequently considered, finer scale step sizes in T did not noticeably improve the resolution of the model curves.

Simplifying assumptions in the models are that mineral surfaces are non-catalytic and that no new H_2 is generated during cooling. The latter assumption is reasonable because H_2 fugacity decreases with T for (mineral) redox buffers applicable to natural hydrothermal systems (e.g., Shock, 1992; Sleep et al., 2004; McDermott et al., 2018), and H_2 generation due to mineral precipitation should be negligible (Seewald and Seyfried, 1990; Seyfried and Ding, 1995). Microbial enhancement of δD_{H2} equilibration rates is well documented, even under scenarios of H_2 consumption, and is considered where fluids have cooled below ~100 °C (Vignais and Billoud, 2007; Campbell et al., 2009; Kawagucci et al., 2011, 2014). Multi-phase behavior is also a complicating factor, although the density dependence of our rate expression makes accounting for this tractable. The density issue is mitigated when considering deep-sea hot springs (Section 4.4) because the overburden of seawater usually exceeds sub-critical vapor pressures during hydrothermal circulation (Bischoff and Rosenbauer, 1985; Bischoff, 1991), and extensive boiling or gas exsolution is uncommon save during eruptions and magmatic events (Von Damm, 2000; Lilley et al., 2003; Seewald et al., 2003; Konno et al., 2006; Lupton et al., 2006; Butterfield et al., 2011; Pester et al., 2014). The density effect on k_1 in submarine settings is therefore minimal compared to continental settings where a low-density steam or gas phase can more easily develop (Fig. 6b). In the latter cases we assume there is no kinetic isotope separation associated with boiling and phase segregation, which might otherwise affect the residual δD_{H2} measured in geothermal liquids/vapors.

4.4. Deep-sea hydrothermal systems

4.4.1. Black smoker vents

Deep sea hydrothermal activity is ubiquitous along mid-ocean ridge and back-arc spreading systems, where seawater circulates close to active magma bodies and reacts with rock at elevated temperatures and pressures (e.g., Edmond et al., 1979; Kelley et al., 2002; Baker and German, 2004; Reeves et al., 2011; German and Seyfried, 2014). Hydrothermal fluids exit the seafloor at temperatures up to ~400 °C, and the hottest of these vents are known as "black smokers", referring to the rapid precipitation of transition metals upon mixing with cold seawater (Haymon, 1983; Tivey et al., 1990). The chemical composition of these fluids, including the H_2 concentration, is a function of T and the lithology of the reacting substrate (Seyfried et al., 1991, 2010, 2015). Previous investigations have demonstrated that α_{OBS} in black smokers appear to be in isotopic equilibrium at T measured during sampling on the seafloor (Horibe and Craig, 1995; Proskurowski et al., 2006; Kawagucci et al., 2010, 2011). The Fe and Mn concentrations, however, indicate fluid–mineral equilibration at higher T, between 400 and 450 °C, which translates to a (roughly) estimated conductive cooling rate of 50 °C/hr (Wilcock, 2004; Pester et al., 2014, 2011). We used this cooling rate to derive a kinetic fractionation trend which assumed initial isotopic equilibrium at 450 °C, and k_1 values at each temperature step were calculated using a near-critical density of 33 mol/L for $T > 373$ °C, transitioning to densities along a 220 bar isopleth for lower temperatures. This approach is consistent with the typical hydrostatic load at 1500 to 3000 m below sea level, and broadly applicable to most deep sea hydrothermal systems.

The resulting model curve is consistent with field data from black smokers, which both indicate the exchange kinetics are fast enough to maintain isotopic equilibrium as end-member fluids cool during ascent to the seafloor for $T > \sim 250$ °C (Fig. 8a).

Fluids exiting the seafloor at lower T predominantly reflect subseafloor mixing between seawater and pure hydrothermal fluid (Edmond et al., 1979; Von Damm and Lilley, 2004; Pester et al., 2008), and the extent of mixing is given by the dissolved Mg concentration, which is effectively zero in the hydrothermal end-member (Von Damm et al., 1985; Seyfried, 1987). Unique datasets presented by Kawagucci et al. (2010, 2011), which report both Mg and δD_{H2} values, demonstrate how such mixing effectively quenches the high-T isotopic signature of the hydrothermal fluid (Fig. 8). However, we note data acquired near the Monju structure of the Kairei vent field (Central-Indian Ridge), and NBC vent in the Iheya North vent field (mid-Okinawa Trough) because these are the only data reported where both low- and high-T fluids were sampled in sufficiently close proximity to possibly share a similar hydrothermal end-member. In both cases, $H_{2(aq)}$ in fluids diffusing from the seafloor surrounding the respective black smokers exhibits lower δD_{H2} with decreasing T. This observation would be expected for fluids approaching equilibrium, but the magnitude of the isotopic shifts is too large to be consistent with the kinetic data at such (low) temperatures. We could find few reasonable combinations of mixing and cooling to explain these observations unless the low-T (mostly seawater) end-member already contained a fraction of $H_{2(aq)}$ in isotopic equilibrium at near ambient conditions (on the order of ~2% of the concentration in the end-member vent fluid). Such a scenario might be consistent with near-equilibrium α_{OBS} values measured in pore fluids of deep-sea sediments (Toki et al., 2011). Regardless of the presence or absence of sediments in near-seafloor flow pathways, these observations from Monju and NBC vent indicate that micro-organisms are likely catalyzing D–H exchange and enhancing the rate of isotopic equilibration. Chemosynthetic microbes are ubiquitous in hydrothermal systems, taking advantage of reduced metals and volatiles for metabolic energy once fluids are mixed to sufficiently low T (e.g., Jannasch and Mottl, 1985; Reysenbach et al., 2006; Orcutt et al., 2011). The data from Monju vent suggest microbial catalysis becomes effective at $T \leq \sim 60$ °C (Fig. 8).

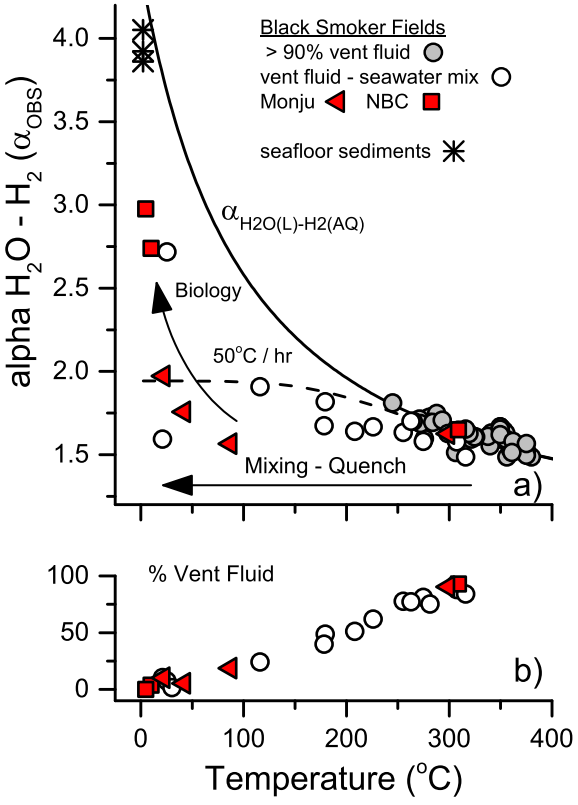

Fig. 8. (a) Measured α_{OBS} vs. measured sampling T in deep-sea (black smoker) hydrothermal fluids (Kawagucci, 2015; Kawagucci et al., 2011, 2016, 2010; Konn et al., 2018; Proskurowski et al., 2006; Welhan and Craig, 1983), compared with equilibrium fractionation ($\alpha_{H2O(L)-H2(AQ)}$, see Fig. 7, Table 2) and a kinetic fractionation trend assuming a cooling rate of 50 °C/hr (dashed). Panel (b) demonstrates how subseafloor mixing between high-T hydrothermal end-member and seawater accounts for lower measured temperatures, which quenches isotopic re-equilibration more rapidly than conductive cooling. Mixing should not affect α_{OBS} because δD_{H2O} of vent fluids and seawater are equivalent (Shanks, 2001). Trend of increasing α_{OBS} for $T < \sim 60$ °C is likely biologically influenced (see Section 4.4.1). Alpha values measured in seafloor sediment pore fluids shown for comparison (Toki et al., 2011).

The biologically enhanced equilibration rate we calculate after Kawagucci et al. (2011) (see Fig. 5) is facilitated by the fact that these researchers collected three gas-tight samples of the same low-T effluent from NBC vent, but they incubated two of the samples for later shipboard processing (remained pressurized, and H_2 dissolved at 25 °C). After 48 hrs they observed the δD_{H2} had shifted from −635‰ (datum shown in Fig. 8) to −736‰ (near equilibrium). These data therefore indicate this naturally occurring microbial assemblage accelerated the D–H exchange of H_2 with water by a factor of ~600× relative to the abiotic rate established in our experiments.

4.4.2. The Lost City hydrothermal system

When compared to the hot/acidic black smokers that typically characterize mid-ocean ridges, hydrothermal effluent of the Lost City vent field reflects different physical and chemical controls (Blackman et al., 2002, 2014; Kelley et al., 2001, 2005; Boschi et al., 2006; Titarenko and McCaig, 2016). At Lost City, H_2-rich fluids with high pH (up to 10.7 at 25 °C) are diffusing out of carbonate-brucite chimneys built upon a fault structure of the Atlantis Massif. Maximum exit temperatures measured during sampling approach 100 °C, and the fluid chemistry indicates deep-seated fluid–mineral reactions at temperatures up to ~250 °C, including a significant contribution from the serpentinization of ultramafic rock (Allen and Seyfried, 2004; Kelley et al., 2005; Foustoukos et al., 2008; Seyfried et al., 2015). Similar to the geochemical controls on black smoker fluid chemistry, these reactions result in the removal of seawater Mg. Despite the lower temperature of the fluids

venting at Lost City, they still contain low dissolved Mg (Lang et al., 2012; Seyfried et al., 2015), indicating the measured temperatures are primarily the result of conductive cooling rather than subseafloor mixing with seawater (cf. Fig. 8).

Hydrogen isotope data from Lost City (Proskurowski et al., 2006) indicate the fluids fall into two groups: (1) those venting at higher T, which have the highest H_2 concentrations and δD_{H2} values, and (2) those venting at (slightly) lower T with lower H_2 concentrations and δD_{H2} values (Fig. 9). The highest T samples, from Beehive vent (91 °C), best represent the (unmixed) hydrothermal end-member of the group 1 fluids (Proskurowski et al., 2006; Lang et al., 2012; Seyfried et al., 2015), and the δD_{H2} values are unlikely to be influenced by microbial activity. We therefore fit cooling models to the measured Beehive T and the range of α_{OBS} measured in the group 1 fluids using constraints similar to those applied to black smoker vents in the previous section. In this case we assumed initial H_2–H_2O isotopic equilibrium at 250 °C, and the best fit to the group 1 data gives a conductive cooling rate of 0.31 to 0.44 °C/hr. The chemistry of the fluids indicates the last T of fluid–mineral equilibration is ~190 °C (Seyfried et al., 2015), and, using this as a benchmark, the cooling rate translates to a residence time of ~11 days in the upflow zone at Lost City.

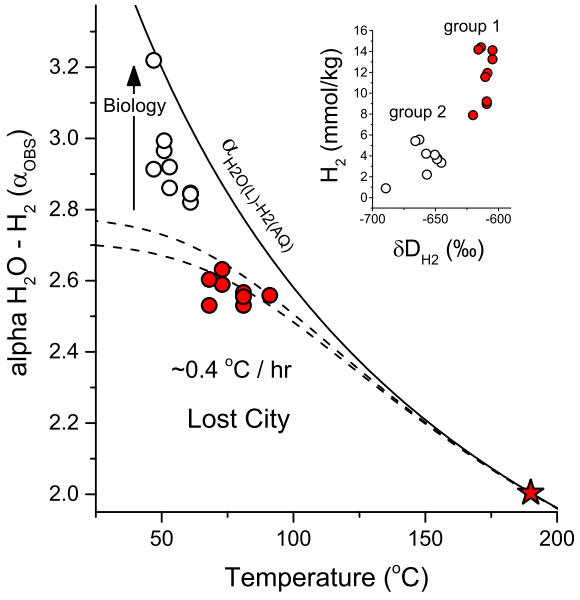

Fig. 9. Measured α_{OBS} vs. measured sampling T in hydrothermal fluids from Lost City vent field (Proskurowski et al., 2006), compared with equilibrium fractionation ($\alpha_{H2O(L)–H2(AQ)}$, see Fig. 7, Table 2), and respective kinetic fractionation trends (dashed) fit to group 1 fluids having higher δD_{H2} and dissolved H_2, and $T > 65$ °C (see inset and Section 4.4.2). Though not appreciably different, T reported here are maximum values from each vent site (Lang et al., 2012) to better account for ambient seawater entrainment during sampling of more diffuse fluids. Kinetic models assumed isotopic equilibrium at 250 °C, and results indicate fluids were still near equilibrium at 190 °C, the apparent T of last fluid–mineral equilibration (star symbol, after Seyfried et al., 2015). Group 2 fluids suggest biologically enhanced rates of isotopic equilibration.

Independent information regarding heat flow and fluid circulation in the Atlantis Massif may be estimated using data from Hole D of IODP Site U1309. Although it is unclear if these observations are analogous to the subseafloor structure directly below Lost City (Blackman et al., 2014; Titarenko and McCaig, 2016), extending the thermal gradient measured in U1309D to 190 °C gives a depth of ~1.75 km below seafloor, which suggests fluids are approaching the seafloor at ~7 m/hr. While this rate has considerable uncertainty, it could be used as a constraint in testing multi-dimensional heat/fluid flow models (e.g., Wanner et al., 2014; Kim et al., 2015).

The group 2 fluids (Fig. 9) discharge at lower temperatures in geographic locations more distal (~50–100 m) to the center of the vent field. This indicates additional conductive cooling occurs in more horizontal flow pathways near the seafloor or within the carbonate structures (Proskurowski et al., 2006; Lang et al., 2012). However, kinetic models fit to the δD_{H2} data of group 2 would require a cooling rate ~5× slower than for group 1, which would imply the group 2 fluids have a substantially different (e.g., more tortuous) upflow pathway. This seems unlikely given both the spatial scale of the vent field, and the modest difference in exit temperatures between the two groups. Another explanation is that group 2 fluids have a longer residence time in flow pathways near the seafloor such that they have cooled to temperatures where microbes begin to thrive and catalyze isotope equilibration. The data of Lang et al. (2012) provide further evidence to support this scenario. These data demonstrate that the group 2 fluids are depleted in both H_2 and sulfate, and enriched in bisulfide, relative to the group 1 fluids, which is consistent with microbial sulfate reduction. Therefore, similar to the mixed fluids of Monju vent (Fig. 8), the Lost City data also suggest that microbial catalysis of H_2–H_2O isotope exchange becomes an important consideration at $T < \sim 60$ °C (Fig. 9).

4.5. Continental volcanic and geothermal systems

The highest temperature field observation for which α_{OBS} is reported comes from degassing magma in the Surtsey Volcano of Iceland (Arnason and Sigurgeirsson, 1968), and these values are indeed consistent with equilibrium at the measured crater T of ~1150 °C (Fig. 10). Other steam and gas dominated fumaroles vent from volcanic terrains at temperatures that extend down to ~100 °C (i.e. boiling at ~1 atm). This broad T range reflects variability in the distance and crustal permeability separating the magmatic heat source and the surface, with the Surtsey magma being an extreme example. Surface exhalations may result from any combination of vapor or liquid dominated flow pathways, depending on geologic and hydrologic controls (White et al., 1971; Truesdell et al., 1977; Fournier, 1989; Lowenstern et al., 2012; Scott et al., 2014, 2015; Harvey et al., 2015). Consequently, relative to the deep-sea systems discussed above, D–H exchange rates in continental systems have more variability, and modeling the cooling history of these fluids has more uncertainty.

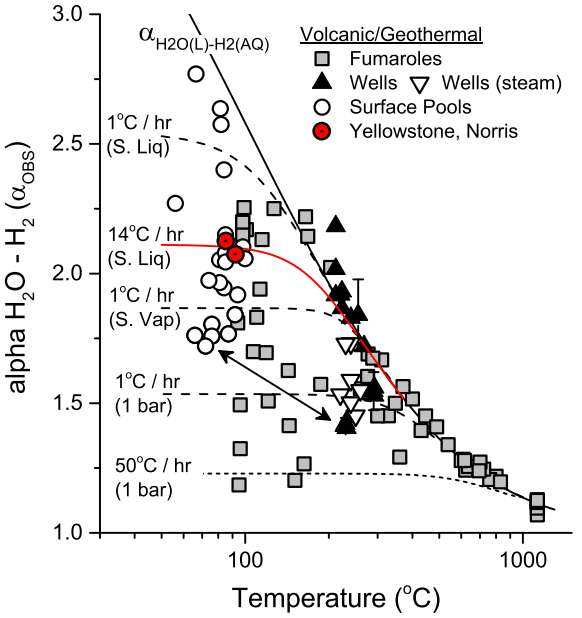

Fig. 10. Measured α_{OBS} vs. measured sampling T from variety of continental volcanic/geothermal settings, compared with $\alpha_{H2O(L)–H2(AQ)}$ equilibrium fractionation ($\alpha_{H2O(v)–H2(g)}$ may be more relevant to fumarole/steam samples, but differs little from $\alpha_{H2O(L)–H2(AQ)}$ over T region shown). Note log T scale. Example kinetic fractionation trends (dashed) are shown for reference, and parentheticals indicate how T - ρ_W dependence was constrained (S. Vap and S. Liq are densities along vapor and liquid branch of H_2O steam saturation curve). Data from Yellowstone (14 °C/hr model fit) are highlighted for discussion (see Section 4.5). Data sources by locality: Iceland (Arnason, 1977; Arnason and Sigurgeirsson, 1968), Japan (Kiyosu, 1983; Kiyosu and Okamoto, 1998; Mizutani, 1983; Tsunogai et al., 2011), Socorro Island (Taran et al., 2010), Kamchatka (Taran et al., 1992), Greece, shallow Aegean Sea (Botz et al., 1996), Yellowstone (Gunter and Musgrave, 1971; Welhan, 1981), New Zealand (Lyon and Hulston, 1984). Of New Zealand samples, measured T not reported for geothermal wells at Wairakei, nor Broadlands, isotopic values were therefore averaged and plotted against known reservoir temperatures, 255 and 290 °C, respectively (Glover and Mroczek, 2009; Simmons et al., 2016). Arrows connect data from Ngawha wells (NZ) and associated surface pools (see Section 4.5).

To evaluate the magnitude of density effects on k_1 (Eq. (17)) we use a cooling rate of 1 °C/hr in three kinetic models where the ρ_W associated with each T is in one case constrained by a constant pressure of 1 bar, and the other models reflect ρ_W along the vapor and liquid branches of the steam saturation curve (Fig. 10, see also Fig. 6b). These models demonstrate that density and cooling rate play equally important roles in determining the temperature trajectory of α_{OBS} in volcanic emissions, and that lower-density vapors and magmatic gases are more likely to preserve T maxima due to relatively sluggish isotope exchange rates, combined with the fact that they cool more rapidly.

Natural geothermal pools have measured temperatures less than 100 °C (Fig. 10), and can be fed by either steam/-gas or liquid emissions (e.g., Sheppard et al., 1992; Lowenstern et al., 2012; Simmons et al., 2005). For example, at Norris Basin in Yellowstone National Park (USA), the fluid T measured at the point of sampling is ~90 °C (Welhan, 1981), having cooled from deeper, hotter conditions between 270 and 340 °C (Fournier, 1989). The dissolved chemistry indicates the fluids feeding Norris are liquids that have undergone periodic boiling during upflow, and likely have lost a fraction of the deeper gas component associated with steam separation (Fournier, 1989). In this case, it is reasonable to model cooling using the T-ρ_W relationship of steam-saturated liquid, because the fluid is likely to follow the boiling curve during upflow once intercepted (Ingebritsen et al., 2010). We assume minimal distillation effects associated with boiling events because the equilibrium values for $H_{2(aq)}$–$H_{2(g)}$ isotope fractionation ($[D/H]_{H2(aq)}/[D/H]_{H2(gas)}$) are much smaller than equilibrium fractionation between H_2 and H_2O, especially for $T > 100$ °C (see Section 4.2, and Fig. S5). Using $\alpha_{H2O(L)–H2(AQ)}$ as the equilibrium reference, the best fit gives a cooling rate of ~14 °C/hr (Fig. 10). Drill-hole measurements from Norris Basin indicate a T of 193 °C at 236 m depth (Bargar and Fournier, 1988), and from this information we derive an average flow rate of ~32 m/hr, which is higher than the value calculated for Lost City (7 m/hr), but of the same magnitude.

Isotope fractionation values (α_{OBS}) measured in liquids recovered from geothermal wells generally show close agreement with equilibrium (Fig. 10). One way to test the validity of using simple cooling models to constrain hydrological characteristics is to compare δD_{H2} measured in natural surface emanations with those obtained from nearby geothermal wells. These wells often extend through lower permeability cap rock and are fed from deeper formations of higher permeability, where convection in the reservoir can produce a relatively uniform vertical temperature distribution on a scale of ~1 km (e.g., Arnórsson, 1995; Cox and Browne, 1998; Garcia et al., 2016). To first order we can conceptualize the system as one where fluids come from a reservoir with a well-defined T that is sufficiently high that H_2 and H_2O are in isotopic equilibrium (typically 200–300 °C, $1/k_1 < 1.3$ hrs), and then cool as they pass through the cap rock to the surface. The only such data currently available for comparison are from the Ngawha geothermal field (NZ), and these appear somewhat anomalous (Lyon and Hulston, 1984), precluding the development of useful kinetic models. The measured reservoir T at Ngawha is ~230 °C (Lyon and Hulston, 1984; Giggenbach et al., 1993; Cox and Browne, 1998), whereas the α_{OBS} values of well fluids and surface pools reflect minimum temperatures of ~440 °C and ~255 °C, respectively (Fig. 10). The difference between these two apparent temperatures is consistent with isotopic re-equilibration as fluids cool during ascent through the cap rock, but it is difficult to explain how both values are higher than the reservoir T. Temperatures exceeding 400 °C are reasonable at depths greater than typical wellbores, having been measured in steam-dominated systems (Garcia et al., 2016). Ngawha, however, is a liquid-dominated system (e.g., Simmons et al., 2016), and the water should boil/convect before achieving such high T unless trapped in tight pore spaces at near-lithostatic pressure, meaning permeability would be inherently low (Johnson and Norton, 1991; Fournier, 1991, 1999). These

constraints do not favor a scenario where gases have moved rapidly between a deeper (higher-T) source region and the drilled reservoir (Lyon and Hulston, 1984). The unexpectedly high δD_{H2} measured also in the Ngawha pools therefore warrants new field investigations here and in other geothermal systems to compare isotope measurements between wells and surface emanations. This may be the best next step in calibrating hydrological models that use D–H exchange kinetics to constrain permeability and flow rate in hydrothermal systems.

4.6. Implications for H_2 generated in low-temperature geologic settings

The models developed in previous sections assume disequilibrium between δD_{H2} and δD_{H2O} observed in hydrothermal solutions largely results from passing through a steep temperature gradient, where cooling occurs faster than the equilibration rate. The H_2 measured in continental shield gases and alkaline springs is likely generated at temperatures well below those driving hydrothermal convection, through processes like serpentinization. Any T-gradients experienced by these fluids will be comparatively mild, and α_{OBS} is typically closer to equilibrium at the T measured during sampling (Fig. 1). However, potential kinetic isotope effects associated with H_2 generation become an important consideration with decreasing T, which could add uncertainty for cooling models applied in lower T settings. The term "kinetic isotope separation factor" (α_{KIE}) is often applied to the fractionation observed when new H_2 is formed from precursor H_2O ($\alpha_{KIE} = [D/H]_{bulk\ H2O}/[D/H]_{new\ H2}$), where α_{KIE} may not be equivalent to $\alpha_{H2O\text{-}H2(eq)}$ at the T and P of formation. For example, if the δD_{H2} of newly-formed H_2 is out of equilibrium with δD_{H2O}, and the associated T is sufficiently low that isotopic equilibration is sluggish, then the simplifying assumption that the kinetic cooling trajectory of α_{OBS} originated on the equilibrium curve ($\alpha_{H2O\text{-}H2(eq)}$) is no longer valid (cf. Fig. 9).

Given kinetic isotope effects may be involved when H_2 is formed at low T, we can use our models to estimate maximum timeframes required to achieve isotopic equilibrium if we assume that H_2 is generated at a constant rate under isothermal conditions. Fluids containing dissolved H_2 liberated from fractures in Precambrian shield rock may represent the closest natural analogue to this scenario (Sherwood Lollar et al., 1993a; Onstott et al., 2006; Sherwood Lollar et al., 2007). Our models assume the α_{KIE} during radiolytic conversion of H_2O to H_2 observed by Lin et al. (2005), who proposed this as a potential mechanism for producing the H_2 observed in deep fracture fluids. They report $\alpha_{KIE} \approx 1.92$ at 25 °C, compared with $\alpha_{H2O(L)\text{–}H2(AQ)} = 3.69$ (equilibrium, 25 °C), which means newly formed H_2 has a δD much higher than is expected for equilibrium the water. For the isothermal kinetic models we use Eq. (17) at $P = 50$ bars for the isotope exchange rates (k_1), which are effectively independent of the low H_2 concentrations in natural fluids, and therefore an arbitrary H_2 generation rate may be used. The models simulate $d[D/H]_{H2}/dt$ as accumulated (bulk) H_2 approaches equilibrium ($\alpha_{H2O(L)\text{–}H2(AQ)}$), concurrent with the constant addition of new H_2 (where $\alpha_{KIE} = 1.92$). The results indicate maximum isothermal residence times (to 97% of equilibrium) of 1.3, 9 and 35 yrs at 50, 25, and 10 °C, respectively. We note, at these temperatures, 97% equates to δD_{H2} being ~8‰ from equilibrium, generally within the reproducibility of field samples.

Although α_{KIE} associated with serpentinization is unknown, currently available data do not suggest H_2 is likely to form any farther from isotopic equilibrium than the value proposed by Lin et al. (2005), either by abiotic or biological mechanisms (Topley and Eyring, 1934; Krichevsky et al., 1961; Roy, 1962; Hammerli et al., 1970; Luo et al., 1991; Stojić et al., 1994; Lin et al., 2005; Walter et al., 2012; Yang et al., 2012). Thus, in general, the timescales required to attain H_2–H_2O isotopic equilibrium in a liquid phase are insignificant relative to residence times of up to millions of years suggested for some fracture fluids (Lippmann et al., 2003; Holland et al., 2013; Kietäväinen et al., 2014). Although, the presence of a gas phase, if possible, would weaken this conclusion somewhat. Overall, isotope fractionation (α_{OBS}) in Precambrian shield gases generally exhibits good agreement with equilibrium (Fig. 1), especially when measured T is well constrained (Onstott et al., 2006).

Biological catalysis of D–H exchange may be another complicating factor in constraining kinetic models of environments associated with low-T H_2 production. The utilization of H_2 is a prevalent metabolic pathway in extreme chemical/physical environments, even where microbial productivity and diversity are low (Schrenk et al., 2004; Nealson et al., 2005; Lin et al., 2006; Onstott et al., 2006; Sherwood Lollar et al., 2007; Toki et al., 2011; Lang et al., 2012; Brazelton et al., 2013; Colwell and D'Hondt, 2013). Cryogenic brine trapped beneath the permanent ice cover of Lake Vida in Antarctica provide an interesting example of isotopic data from an extreme environment ($\delta D_{H2} = -704$‰, $\delta D_{H2O} = -250$‰ at −13.4 °C). The δD_{H2} is far from equilibrium ($\alpha_{OBS} = 2.567$, Fig. 1) despite the presence of a (slow) bacterial ecosystem (Murray et al., 2012). The brine appears to have been geochemically isolated for ~2,800 yrs, and Murray et al. (2012) note the mechanism of H_2 production and the effect of microbes on C-H-N-S isotope systematics are both poorly constrained. If we extend to −13.4 °C our model for estimating maximum (isothermal) residence times, the results indicate δD_{H2} should reach equilibrium within ~350 yrs. This is shorter than the reported timeframe of isolation by an order of magnitude. Therefore, should these Lake Vida data prove reproducible, the observed disequilibrium seems to require a mechanism of H_2 removal that rivals the rate of production, and a kinetic isotope effect associated with this process. For example, if we assume microbial activity only moves δD_{H2} towards equilibrium (Romanek et al., 2003; Valentine et al., 2004; Campbell et al., 2009; Yang et al., 2012; Kawagucci et al., 2014; Okumura et al., 2016), a low degree of biological activity may allow isotopically lighter H_2 to preferentially diffuse away through the ice (Strauss et al., 1994). Thus, especially in cool or isolated geologic settings, representative isotope exchange models may need to account for additional (physical) mechanisms

that could impose kinetic isotope separation, such as degassing or diffusion. In turn, such models might elucidate better the impact of biology on D/H isotope systematics in extreme natural environments, with potential implications for identifying bio-signatures elsewhere in the solar system.

5. CONCLUSIONS

Combining new and historical experimental data, we have derived a simple, but broadly applicable rate law to describe the D–H exchange rate (k) between H_2 and H_2O as the system approaches isotopic equilibrium. If species concentrations are cast in units of [mol/L], good agreement is observed when comparing the results of liquid phase experiments, reported here, to those of gas phase experiments previously reported by Lecluse and Robert (1994). First-order exchange rates (k_1, units hr^{-1}) may be calculated by constraining T and the concentrations [H_2] and [H_2O], both in mol/L, at the associated P of interest. The result is a density-dependent rate expression that can easily account for phase changes that commonly occur in evolving geological systems. The new experimental data also help constrain equilibrium isotope fractionation for H_2 dissolved in liquid water, and we report updated polynomials to describe the T dependence of $\alpha_{H2O\text{-}H2(eq)}$ in the H_2–H_2O system.

Isotope fractionation between H_2 and H_2O (α_{OBS}) is considered an important indicator of the temperature history of naturally occurring fluids/gases. Historical field data concur with our experimentally-derived rates, indicating D–H exchange kinetics are sufficiently fast in liquid water that $\alpha_{H2O\text{-}H2}$ temperatures usually reflect equilibrium when T measured during sampling exceeds ~250 °C. (e.g., Fig. 8). For liquid-phase solutions, such temperatures are below the near-critical limit of hydrothermal convection. In such cases, as we have attempted to demonstrate, isotopic equilibrium ($\alpha_{H2O\text{-}H2(eq)}$) at these high-temperature conditions provides a relatively unambiguous starting point for simple kinetic models that assume the degree of disequilibrium observed in natural fluids is a function of the cooling rate. The H_2–H_2O system appears uniquely sensitive in a temperature range ideal for estimating transit times of upwardly-advecting hydrothermal solutions. Both T and density ($\sim\rho_W$) have a significant effect on the D–H exchange rate, which explains the greater variability and relatively high $\alpha_{H2O\text{-}H2}$ temperatures reflected in steam discharges and fumarolic gases (e.g., Fig. 10).

Steep temperature gradients and relatively rapid cooling associated with hydrothermal convection facilitate a greater degree of isotopic disequilibrium than is observed in alkaline spring waters and Precambrian fracture fluids. In these systems, H_2 formation may occur at relatively low temperatures (<100 °C), which increases the probability that factors other than cooling may have affected the observed δD_{H2}. When applied to hydrothermal fluids, kinetic cooling models indicate microbiomes must enhance rates of isotopic re-equilibration at $T < \sim 60$ °C. In low-T discharges, where a high-T origin of H_2 cannot be assumed, it is more difficult to demonstrate the biological effects. There is an additional possibility that δD_{H2} can include a kinetic isotope effect associated with H_2 generation. In this case, disequilibrium could be observed even if H_2 formed at the T measured during sampling, although our models suggest isotopic equilibrium would be established within 1.3, 9 and 35 yrs at 50, 25, and 10 °C, respectively.

ACKNOWLEDGEMENTS

We would like to thank Daniel Stolper, Stuart Simmons, Ben Tutolo and Pat Dobson for thoughtful discussions that contributed to the scope of the original manuscript. We also thank Matthew Fantle and three anonymous reviewers, whose comments greatly improved the clarity and content of this publication. This work was supported by the U.S. Department of Energy, Office of Science, Office of Basic Energy Sciences, Chemical Sciences, Geosciences, and Biosciences Division, under Award Number DE-AC02-05CH11231.

APPENDIX A. SUPPLEMENTARY MATERIAL

Supplementary data to this article can be found online at https://doi.org/10.1016/j.gca.2018.09.015.

REFERENCES

Abrajano T. A., Sturchio N. C., Kennedy B. M., Lyon G. L., Muehlenbachs K. and Bohlke J. K. (1990) Geochemistry of reduced gas related to serpentinization of the Zambales ophiolite. *Philippines. Appl. Geochem.* **5**, 625–630.

Ahlbom, K., Olsson, O., Sehlstedt, S., 1995. Temperature conditions in the SKB study sites. Svensk Kärnbränslehantering AB, Tech. Rep. 95-16.

Albertsson T., Semenov D. and Henning T. (2014) Chemodynamical deuterium fractionation in the early solar nebula: the origin of water on Earth and in asteroids and comets. *Astrophys. J.* **784**. https://doi.org/10.1088/0004-1637X/1784/1081/1039.

Allen D. E. and Seyfried, Jr., W. E. (2004) Serpentinization and heat generation: constraints from Lost City and Rainbow hydrothermal systems. *Geochim. Cosmochim. Acta* **68**, 1347–1354.

Arnason B. (1977) The hydrogen-water isotope thermometer applied to geothermal areas in Iceland. *Geothermics* **5**, 75–80.

Arnason B. and Sigurgeirsson T. (1968) Deuterium content of water vapor and hydrogen in volcanic gas at Surtsey, Iceland. *Geochim. Cosmochim. Acta* **32**, 807–813.

Arnórsson S. (1995) Geothermal systems in Iceland: structure and conceptual models—I. High-temperature areas. *Geothermics* **24**, 561–602.

Baker E. T. and German C. R. (2004) On the global distribution of hydrothermal vent fields. In *Mid-Ocean Ridges: Hydrothermal Interactions Between the Lithosphere and Oceans, Geophys. Monogr. Ser., 148* (eds. C. R. German, J. Lin and L. M. Parson). AGU, pp. 245–266.

Bardo R. D. and Wolfsberg M. (1976) A theoretical calculation of the equilibrium constant for the isotopic exchange reaction between H_2O and HD. *J. Phys. Chem.* **80**, 1068–1071.

Bargar K. E. and Fournier R. O. (1988) Effects of glacial ice on subsurface temperatures of hydrothermal systems in Yellowstone National Park, Wyoming: fluid-inclusion evidence. *Geology* **16**, 1077–1080.

Barnes I., O'Neil J. R. and Trescases J. J. (1978) Present day serpentinization in New Caledonia, Oman and Yugoslavia. *Geochim. Cosmochim. Acta* **42**, 144–145.

Berndt M. E., Allen D. E. and Seyfried, Jr., W. E. (1996a) Reduction of CO_2 during serpentinization of olivine at 300°C and 500 bar. *Geology* **24**, 351–354.

Berndt M. E., Seal, II, R. R., Shanks, III, W. C. and Seyfried, Jr., W. E. (1996b) Hydrogen isotope systematics of phase separation in submarine hydrothermal systems: experimental calibration and theoretical models. *Geochim. Cosmochim. Acta* **60**, 1595–1604.

Bischoff J. L. (1991) Densities of liquids and vapors in boiling NaCl-H_2O solutions: a PVTx summary from 300° to 500°C. *Am. J. Sci.* **291**, 309–338.

Bischoff J. L. and Rosenbauer R. J. (1985) An empirical equation of state for hydrothermal seawater (3.2% NaCl). *Am. J. Sci.* **285**, 725–763.

Blackman D. K., Slagle A., Guerin G. and Harding A. (2014) Geophysical signatures of past and present hydration within a young oceanic core complex. *Geophys. Res. Lett.* **41**, 1179–1186.

Blackman D. K., Karson J. A., Kelley D. S., Cann J. R., Früh-Green G. L., Gee J. S., Hurst S. D., John B. E., Morgan J., Nooner S. L., Ross D. K., Schroeder T. J. and Williams E. A. (2002) Geology of the Atlantis Massif (Mid-Atlantic Ridge, 30° N): Implications for the evolution of an ultramafic oceanic core complex. *Mar. Geophys. Res.* **23**, 443–469.

Boschi C., Fruh-Green G. L., Delacour A., Karson J. A. and Kelley D. S. (2006) Mass transfer and fluid flow during detachment faulting and development of an oceanic core complex, Atlantis Massif (MAR 30°N). *Geochem. Geophys. Geosyst.* **7**, Q01004, doi: 01010.01029/02005GC001074.

Botz R., Stüben D., Winckler G., Bayer R., Schmitt M. and Faber E. (1996) Hydrothermal gases offshore Milos Island, Greece. *Chem. Geol.* **130**, 161–173.

Brazelton W. J., Morrill P. L., Szponar N. and Schrenk M. O. (2013) Bacterial communities associated with subsurface geochemical processes in continental serpentinite springs. *Appl. Environ. Microbiol.* **79**, 3906–3916.

Butterfield D. A., Nakamura K., Takano B., Lilley M. D., Lupton J. E., Resing J. A. and Roe K. K. (2011) High SO_2 flux, sulfur accumulation, and gas fractionation at an erupting submarine volcano. *Geology* **39**, 803–806.

Campbell B. J., Li C., Sessions A. L. and Valentine D. L. (2009) Hydrogen isotopic fractionation in lipid biosynthesis by H_2-consuming *Desulfobacterium autotrophicum*. *Geochim. Cosmochim. Acta* **73**, 2744–2757.

Cardace D., Meyer-Dombard D. A. R., Woycheese K. M. and Arcilla C. A. (2015) Feasible metabolisms in high pH springs of the Philippines. *Front. Microbiol.* **6**, 10.

Charlou J. L., Donval J. P., Fouquet Y., Jean-Baptiste P. and Holm N. (2002) Geochemistry of high H_2 and CH_4 vent fluids issuing from ultramafic rocks at the Rainbow hydrothermal field (36°14'N, MAR). *Chem. Geol.* **191**, 345–359.

Chiodini G. and Marini L. (1998) Hydrothermal gas equilibria: the H_2O-H_2-CO_2-CO-CH_4 system. *Geochim. Cosmochim. Acta* **62**, 2673–2687.

Cole D. R. and Chakraborty S. (2001) Rates and mechanisms of isotopic exchange. In *Stable Isotope Geochemistry, Rev. Mineral. Geochem. 43* (eds. J. W. Valley and D. R. Cole). MSA, Chantilly, VA, pp. 83–223.

Colwell F. S. and D'Hondt S. (2013) Nature and extent of the deep biosphere. In *Carbon in the Earth, Rev. Min. Geochem. 75* (eds. R. M. Hazen, A. P. Jones and J. A. Baross). MSA, pp. 547–574.

Coveney, Jr., R. M., Goebel E. D., Zeller E. J., Dreschhoff G. A. M. and Angino E. E. (1987) Serpentinization and the origin of hydrogen gas in Kansas. *Am. Assoc. Petr. Geol. B.* **71**, 39–48.

Cox M. E. and Browne P. (1998) Hydrothermal alteration mineralogy as an indicator of hydrology at the Ngawha geothermal field, New Zealand. *Geothermics* **27**, 259–270.

Craig H. (1961) Standard for reporting concentrations of deuterium and oxygen-18 in natural waters. *Science* **133**, 1833–1834.

Criss R. E. (1999) *Principles of Stable Isotope Distribution*. Oxford University Press.

Criss R. E., Gregory R. T. and Taylor, Jr., H. P. (1987) Kinetic theory of oxygen isotopic exchange between minerals and water. *Geochim. Cosmochim. Acta* **51**, 1099–1108.

D'Amore F. and Panichi C. (1980) Evaluation of deep temperatures of hydrothermal systems by a new gas geothermometer. *Geochim. Cosmochim. Acta* **44**, 549–556.

Drummond S. E. and Ohmoto H. (1985) Chemical evolution and mineral deposition in boiling hydrothermal systems. *Econ. Geol.* **80**, 126–147.

Edmond J. M., Measures C., McDuff R. E., Chan L., Collier R., Grant B., Gordon L. I. and Corliss J. (1979) Ridge crest hydrothermal activity and the balances of the major and minor elements in the ocean: the Galapagos data. *Earth Planet. Sci. Lett.* **46**, 1–18.

Etiope G., Samardzic N., Grassa F., Hrvatovic H., Miosic N. and Skopljak F. (2017) Methane and hydrogen in hyperalkaline groundwaters of the serpentinized Dinaride ophiolite belt, Bosnia and Herzegovina. *Appl. Geochem.* **84**, 286–296.

Fernandez-Prini R., Alvarez J. L. and Harvey A. H. (2003) Henry's constants and vapor-liquid distribution constants for gaseous solutes in H_2O and D_2O at high temperatures. *J. Phys. Chem. Ref. Data* **32**, 903–916.

Flournoy J. M. and Wilmarth W. K. (1961) The base catalyzed exchange of hydrogen gas and protonic solvents. III. The catalytic efficiency of concentrated aqueous alkali. *J. Am. Chem. Soc.* **83**, 2257–2262.

Fournier R. O. (1989) Geochemistry and dynamics of the Yellowstone National Park hydrothermal system. *Annu. Rev. Earth Planet. Sci.* **17**, 13–53.

Fournier R. O. (1991) The transition from hydrostatic to greater than hydrostatic fluid pressure in presently active continental hydrothermal systems in crystalline rock. *Geophys. Res. Lett.* **18**, 955–958.

Fournier R. O. (1999) Hydrothermal processes related to movement of fluid from plastic into brittle rock in the magmatic-epithermal environment. *Econ. Geol.* **94**, 1193–1211.

Foustoukos D. I. and Mysen B. O. (2012) D/H fractionation in the H_2–H_2O system at supercritical water conditions: compositional and hydrogen bonding effects. *Geochim. Cosmochim. Acta* **86**, 88–102.

Foustoukos D. I., Savov I. P. and Janecky D. R. (2008) Chemical and isotopic constraints on water/rock interactions at the Lost City hydrothermal field, 30°N Mid-Atlantic Ridge. *Geochim. Cosmochim. Acta* **72**, 5457–5474.

Friedman I. (1953) Deuterium content of natural waters and other substances. *Geochim. Cosmochim. Acta* **4**, 89–103.

Friedman I. and O'Neil J. R. (1977) Compilation of stable isotope fractionation factors of geochemical interest. Data of Geochemistry, U.S. Geol. *Surv. Prof. Paper*, 440.

Fritz P., Clark I. D., Fontes J.-C., Whiticar M. J. and Faber E. (1992) *Deuterium and ^{13}C evidence for low temperature production of hydrogen and methane in a highly alkaline groundwater environment in Oman*. Balkema, Rotterdam, pp. 793–796.

Fu Q., Lollar B. S., Horita J., Lacrampe-Couloume G. and Seyfried, Jr., W. E. (2007) Abiotic formation of hydrocarbons under hydrothermal conditions: constraints from chemical and isotope data. *Geochim. Cosmochim. Acta* **71**, 1982–1998.

Gallant R. M. and Von Damm K. L. (2006) Geochemical controls on the hydrothermal fluids from the Kairei and Edmond Vent Fields, 23°–25°S, Central Indian Ridge. *Geochem. Geophys. Geosyst.* **7**, Q06018.

Garcia J., Hartline C., Walters M., Wright M., Rutqvist J., Dobson P. F. and Jeanne P. (2016) The Northwest Geysers EGS Demonstration Project, California: Part 1: Characterization and reservoir response to injection. *Geothermics* **63**, 97–119.

Genda H. and Ikoma M. (2008) Origin of the ocean on the Earth: early evolution of water D/H in a hydrogen-rich atmosphere. *Icarus* **194**, 42–52.

German C. R. and Seyfried, Jr., W. E. (2014) Hydrothermal processes. In *Treatise on Geochemistry, vol. 8: The Oceans and Marine Geochemistry* (ed. S. A. Elias). Elsevier, pp. 191–233.

Giggenbach W. F. (1987) Redox processes governing the chemistry of fumarolic gas discharges from White Island, New Zealand. *Appl. Geochem.* **2**, 143–161.

Giggenbach W. F. (1997) The origin and evolution of fluids in magmatic-hydrothermal systems. In *Geochemistry of Hydrothermal Ore Deposits* (ed. H. L. Barnes), third ed. John Wiley & Sons Inc, pp. 737–796.

Giggenbach W. F., Sano Y. and Wakita H. (1993) Isotopic composition of helium, and CO_2 and CH_4 contents in gases produced along the New Zealand part of a convergent plate boundary. *Geochim. Cosmochim. Acta* **57**, 3427–3455.

Glover R. B. and Mroczek E. K. (2009) Chemical changes in natural features and well discharges in response to production at Wairakei, New Zealand. *Geothermics* **38**, 117–133.

Gunter B. D. and Musgrave B. C. (1971) New evidence on the origin of methane in hydrothermal gases. *Geochim. Cosmochim. Acta* **35**, 113–118.

Hammerli M., Mislan J. P. and Olmstead W. J. (1970) Effect of overpotential on the temperature dependence of the electrolytic hydrogen-deuterium separation factor on platinum. *J. Electrochem. Soc.* **117**, 751–757.

Harvey M. C., Rowland J. V., Chiodini G., Rissmann C. F., Bloomberg S., Hernández P. A., Mazot A., Viveiros F. and Werner C. (2015) Heat flux from magmatic hydrothermal systems related to availability of fluid recharge. *J. Volcanol. Geoth. Res.* **302**, 225–236.

Haymon R. (1983) Growth history of hydrothermal black smoker chimneys. *Nature* **301**, 695–698.

Hilkert A. W., Douthitt C. B., Schlüter H. J. and Brand W. A. (1999) Isotope ratio monitoring gas chromatography/mass spectrometry of D/H by high temperature conversion isotope ratio mass spectrometry. *Rapid Commun. Mass Spectrom.* **13**, 1226–1230.

Holland G., Lollar B. S., Li L., Lacrampe-Couloume G., Slater G. F. and Ballentine C. J. (2013) Deep fracture fluids isolated in the crust since the Precambrian era. *Nature* **497**, 357–360.

Horibe Y. and Craig H. (1995) D/H fractionation in the system methane-hydrogen-water. *Geochim. Cosmochim. Acta* **59**, 5209–5217.

Horita J. and Wesolowski D. J. (1994) Liquid-vapor fractionation of oxygen and hydrogen isotopes of water from the freezing to the critical temperature. *Geochim. Cosmochim. Acta* **58**, 3425–3437.

Hsu H.-W., Postberg F., Sekine Y., Shibuya T., Kempf S., Horányi M., Juhász A., Altobelli N., Suzuki K., Masaki Y., Kuwatani T., Tachibana S., Sirono S.-I., Moragas-Klostermeyer G. and Srama R. (2015) Ongoing hydrothermal activities within Enceladus. *Nature* **519**, 207.

Ingebritsen S. E., Geiger S., Hurwitz S. and Driesner T. (2010) Numerical simulation of magmatic hydrothermal systems. *Rev. Geophys.* **48**, RG1002. https://doi.org/10.10.1029/2009RG000287.

Jannasch H. W. and Mottl M. J. (1985) Geomicrobiology of deep-sea hydrothermal vents. *Science* **229**, 717–725.

Jeffrey A. W. A. and Kaplan I. R. (1988) Hydrocarbons and inorganic gases in the Gravberg-1 well, Siljan Ring, Sweden. *Chem. Geol.* **71**, 237–255.

Jessop A. M. and Lewis T. (1978) Heat flow and heat generation in the Superior Province of the Canadian Shield. *Tectonophysics* **50**, 55–77.

Johnson J. W. and Norton D. (1991) Critical phenomena in hydrothermal systems: state, thermodynamic, electrostatic, and transport properties of H_2O in the critical region. *Am. J. Sci.* **291**, 541–648.

Juhlin C., Wallroth T., Smellie J., Eliasson T., Ljunggren C., Leijon B. and Beswick J. (1998) *The Very Deep Hole Concept: Geoscientific Appraisal of Conditions at Great Depth*. Svensk Kärnbränslehantering AB, SKB-TR-98-05.

Kawagucci S. (2015) Fluid geochemistry of high-temperature hydrothermal fields in the Okinawa Trough. In *Subseafloor Biosphere Linked to Hydrothermal Systems: TAIGA Concept* (eds. J.-. I. Ishibashi, K. Okino and M. Sunamura). Springer, pp. 387–403.

Kawagucci S., Toki T., Ishibashi J.-I., Takai K., Ito M., Oomori T. and Gamo T. (2010) Isotopic variation of molecular hydrogen in 20°–375°C hydrothermal fluids as detected by a new analytical method. *J. Geophys. Res.* **115**, G03021, doi: 03010.01029/02009JG001203.

Kawagucci S., Kobayashi M., Hattori S., Yamada K., Ueno Y., Takai K. and Yoshida N. (2014) Hydrogen isotope systematics among H_2–H_2O–CH_4 during the growth of the hydrogenotrophic methanogen *Methanothermobacter thermautotrophicus* strain ΔH. *Geochim. Cosmochim. Acta* **142**, 601–614.

Kawagucci S., Chiba H., Ishibashi J.-I., Yamanaka T., Toki T., Muramatsu Y., Ueno Y., Makabe A., Inoue K., Yoshida N., Nakagawa S., Nunoura T., Takai K., Takahata N., Sano Y., Narita T., Teranishi G., Obata H. and Gamo T. (2011) Hydrothermal fluid geochemistry at the Iheya North field in the mid-Okinawa Trough: implication for origin of methane in subseafloor fluid circulation systems. *Geochem. J.* **45**, 109–124.

Kawagucci S., Miyazaki J., Noguchi T., Okamura K., Shibuya T., Watsuji T., Nishizawa M., Watanabe H., Okino K., Takahata N., Sano Y., Nakamura K., Shuto A., Abe M., Takaki Y., Nunoura T., Koonjul M., Singh M., Beedessee G., Khishma M., Bhoyroo V., Bissessur D., Kumar L. S., Marie D., Tamaki K. and Takai K. (2016) Fluid chemistry in the Solitaire and Dodo hydrothermal fields of the Central Indian Ridge. *Geofluids* **16**. https://doi.org/10.1111/gfl.12201.

Kelley D. S., Baross J. A. and Delaney J. R. (2002) Volcanoes, fluids, and life at mid-ocean ridge spreading centers. *Annu. Rev. Earth Planet. Sci.* **30**, 385–491.

Kelley D. S., Karson J. A., Blackman D. K., Fruh-Green G. L., Butterfield D. A., Lilley M. D., Olson E. J., Schrenk M. O., Roe K. K., Lebon G. T. and Rivizzigno P. (2001) An off-axis hydrothermal vent field near the Mid-Atlantic Ridge at 30°N. *Nature* **412**, 145–149.

Kelley D. S., Karson J. A., Früh-Green G. L., Yoerger D. R., Shank T. M., Butterfield D. A., Hayes J. M., Schrenk M. O., Olson E. J., Proskurowski G., Jakuba M., Bradley A., Larson B., Ludwig K., Glickson D., Buckman K., Bradley A. S., Brazelton W. J., Roe K., Elend M. J., Delacour A., Bernasconi S. M., Lilley M. D., Baross J. A., Summons R. E. and Sylva S. P. (2005) A serpentinite-hosted ecosystem: the lost city hydrothermal field. *Science* **307**, 1428–1434.

Kietäväinen R., Ahonen L., Kukkonen I. T., Niedermann S. and Wiersberg T. (2014) Noble gas residence times of saline waters within crystalline bedrock, Outokumpu Deep Drill Hole, Finland. *Geochim. Cosmochim. Acta* **145**, 159–174.

Kietäväinen R., Ahonen L., Niinikoski P., Nykänen H. and Kukkonen I. T. (2017) Abiotic and biotic controls on methane formation down to 2.5 km depth within the Precambrian Fennoscandian Shield. *Geochim. Cosmochim. Acta* **202**, 124–145.

Kim J., Sonnenthal E. and Rutqvist J. (2015) A sequential implicit algorithm of chemo-thermo-poro-mechanics for fractured geothermal reservoirs. *Comp. Geosci.* **76**, 59–71.

Kishima N. (1989) A thermodynamic study on the pyrite-pyrrhotite-magnetite-water system at 300–500°C with relevance to the fugacity/concentration quotient of aqueous H_2S. *Geochim. Cosmochim. Acta* **53**, 2143–2155.

Kishima N. and Sakai H. (1984) Fugacity-concentration relationship of dilute hydrogen in water at elevated temperature and pressure. *Earth Planet. Sci. Lett.* **67**, 79–86.

Kita A., Matsuo S., Wakita H. and Nakamura Y. (1980) D/H ratios of H_2 in soil gases as an indicator of fault movements. *Geochem. J.* **14**, 317–320.

Kiyosu Y. (1983) Hydrogen isotopic compositions of hydrogen and methane from some volcanic areas in northeastern Japan. *Earth Planet. Sci. Lett.* **62**, 41–52.

Kiyosu Y. and Okamoto Y. (1998) Variation in fumarolic H_2 gas and volcanic activity at Nasudake in Japan. *J. Volcanol. Geoth. Res.* **80**, 27–37.

Klein F., Grozeva N. G., Seewald J. S., McCollom T. M., Humphris S. E., Moskowitz B., Berquó T. S. and Kahl W.-A. (2015) Experimental constraints on fluid-rock reactions during incipient serpentinization of harzburgite. *Am. Mineral.* **100**, 991–1002.

Knox M., Quay P. D. and Wilbur D. (1992) Kinetic isotopic fractionation during air-water gas transfer of O_2, N_2, CH_4, and H_2. *J. Geophys. Res.* **97**, 20335–20343.

Komor S. C., Valley J. W. and Brown P. E. (1988) Fluid-inclusion evidence for impact heating at the Siljan Ring, Sweden. *Geology* **16**, 711–715.

Konn C., Donval J. P., Guyader V., Roussel E., Fourre E., Jean-Baptiste P., Pelleter E., Charlou J. L. and Fouquet Y. (2018) Organic, gas, and element geochemistry of hydrothermal fluids of the newly discovered extensive hydrothermal area in the Wallis and Futuna region (SW Pacific). *Geofluids* **2018**. https://doi.org/10.1155/2018/7692839.

Konno U., Tsunogai U., Nakagawa F., Nakaseama M., Ishibashi J.-I., Nunoura T. and Nakamura K.-I. (2006) Liquid CO_2 venting on the seafloor: Yonaguni Knoll IV hydrothermal system, Okinawa Trough. *Geophys. Res. Lett.* **33**, L16607. https://doi.org/10.1029/2006GL026115.

Krichevsky M. I., Friedman I., Newell M. F. and Sisler F. D. (1961) Deuterium fractionation during molecular hydrogen formation in a marine pseudomonad. *J. Biol. Chem.* **236**, 2520–2525.

Lang S. Q., Früh-Green G. L., Bernasconi S. M., Lilley M. D., Proskurowski G., Méhay S. and Butterfield D. A. (2012) Microbial utilization of abiogenic carbon and hydrogen in a serpentinite-hosted system. *Geochim. Cosmochim. Acta* **92**, 82–99.

Lasaga A. C. (1998) *Kinetic Theory in Earth Sciences*. Princeton University Press.

Lecluse C. and Robert F. (1994) Hydrogen isotope exchange reaction rates: origin of water in the inner solar system. *Geochim. Cosmochim. Acta* **58**, 2927–2939.

Lemke K. H., Rosenbauer R. J. and Bird D. K. (2009) Peptide synthesis in early Earth hydrothermal systems. *Astrobiology* **9**, 141–146.

Lilley M. D., Lupton J. E., Butterfield D. A. and Olson E. (2003) Magmatic events can produce rapid changes in hydrothermal vent chemistry. *Nature* **422**, 878–881.

Lin L.-H., Slater G. F., Sherwood Lollar B., Lacrampe-Couloume G. and Onstott T. C. (2005) The yield and isotopic composition of radiolytic H_2, a potential energy source for the deep subsurface biosphere. *Geochim. Cosmochim. Acta* **69**, 893–903.

Lin L.-H., Wang P.-L., Rumble D., Lippmann-Pipke J., Boice E., Pratt L. M., Lollar B. S., Brodie E. L., Hazen T. C., Andersen G. L., DeSantis T. Z., Moser D. P., Kershaw D. and Onstott T. C. (2006) Long-term sustainability of a high-energy, low-diversity crustal biome. *Science* **314**, 479–482.

Lippmann J., Stute M., Torgersen T., Moser D. P., Hall J. A., Lin L., Borcsik M., Bellamy R. E. S. and Onstott T. C. (2003) Dating ultra-deep mine waters with noble gases and ^{36}Cl, Witwatersrand Basin, South Africa. *Geochim. Cosmochim. Acta* **67**, 4597–4619.

Lowenstern J. B., Bergfeld D., Evans W. C. and Hurwitz S. (2012) Generation and evolution of hydrothermal fluids at Yellowstone: insights from the Heart Lake Geyser Basin. *Geochem. Geophys. Geosyst.* **13**, Q01017, doi: 01010.01029/02011GC003835.

Luo Y.-H., Sternberg L., Suda S., Kumazawa S. and Mitsui A. (1991) Extremely low D/H ratios of photoproduced hydrogen by cyanobacteria. *Plant Cell Physiol.* **32**, 897–900.

Lupton J., Butterfield D., Lilley M., Evans L., Nakamura K.-I., Chadwick W., Resing J., Embley R., Olson E., Proskurowski G., Baker E., de Ronde C., Roe K., Greene R., Lebon G. and Young C. (2006) Submarine venting of liquid carbon dioxide on a Mariana Arc volcano. *Geochem. Geophys. Geosyst.* **7**, Q08007. https://doi.org/10.1029/2005GC001152.

Lyon G. L. and Hulston J. R. (1984) Carbon and hydrogen isotopic compositions of New Zealand geothermal gases. *Geochim. Cosmochim. Acta* **48**, 1161–1171.

Marsic N. and Grundfelt B. (2013) *Review of Geoscientific Data of Relevance to Disposal of Spent Nuclear Fuel in Deep Boreholes in Crystalline Rock*. Svensk Kärnbränslehantering AB, SKB-P-13-12.

Mayhew L. E., Ellison E. T., McCollom T. M., Trainor T. P. and Templeton A. S. (2013) Hydrogen generation from low-temperature water–rock reactions. *Nat. Geosci.* **6**, 478–484.

McCollom T. M., Klein F., Robbins M., Moskowitz B., Berquó T. S., Jöns N., Bach W. and Templeton A. (2016) Temperature trends for reaction rates, hydrogen generation, and partitioning of iron during experimental serpentinization of olivine. *Geochim. Cosmochim. Acta* **181**, 175–200.

McDermott J. M., Seewald J. S., German C. R. and Sylva S. P. (2015) Pathways for abiotic organic synthesis at submarine hydrothermal fields. *Proc. Natl. Acad. Sci. USA* **112**, 7668–7672.

McDermott J. M., Sylva S. P., Ono S., German C. R. and Seewald J. S. (2018) Geochemistry of fluids from Earth's deepest ridge-crest hot-springs: Piccard hydrothermal field, Mid-Cayman Rise. *Geochim. Cosmochim. Acta* **228**, 95–118.

Miller S. L. and Rittenberg D. (1958) The catalysis of the H_2–D_2O exchange by aqueous buffer solutions. *J. Am. Chem. Soc.* **80**, 64–65.

Miller H. M., Matter J. M., Kelemen P., Ellison E. T., Conrad M. E., Fierer N., Ruchala T., Tominaga M. and Templeton A. S. (2016) Modern water/rock reactions in Oman hyperalkaline peridotite aquifers and implications for microbial habitability. *Geochim. Cosmochim. Acta* **179**, 217–241.

Mizutani Y. (1983) Deuterium fractionation between water vapor and hydrogen gas in fumarolic gases. *Geochem. J.* **17**, 161–164.

Morrison J., Brockwell T., Merren T., Fourel F. and Phillips A. M. (2001) On-line high-precision stable hydrogen isotopic analyses on nanoliter water samples. *Anal. Chem.* **73**, 3570–3575.

Muccitelli J. and Wen W.-Y. (1978) Solubilities of hydrogen and deuterium gases in water and their isotope fractionation factor. *J. Sol. Chem.* **7**, 257–267.

Murray A. E., Kenig F., Fritsen C. H., McKay C. P., Cawley K. M., Edwards R., Kuhn E., McKnight D. M., Ostrom N. E., Peng V., Ponce A., Priscu J. C., Samarkin V., Townsend A. T., Wagh P., Young S. A., Yung P. T. and Doran P. T. (2012) Microbial life at −13 °C in the brine of an ice-sealed Antarctic lake. *Proc. Natl. Acad. Sci. USA* **109**, 20626–20631.

Neal C. and Stanger G. (1983) Hydrogen generation from mantle source rocks in Oman. *Earth Planet. Sci. Lett.* **66**, 315–320.

Nealson K. H., Inagaki F. and Takai K. (2005) Hydrogen-driven subsurface lithoautotrophic microbial ecosystems (SLiMEs): do they exist and why should we care? *Trends Microbiol.* **13**, 405–410.

Niemann H. B., Atreya S. K., Demick J. E., Gautier D., Haberman J. A., Harpold D. N., Kasprzak W. T., Lunine J. I., Owen T. C. and Raulin F. (2010) Composition of Titan's lower atmosphere and simple surface volatiles as measured by the Cassini-Huygens probe gas chromatograph mass spectrometer experiment. *J. Geophys. Res.* **115**, EI2006, doi: 2010.1029/2010JE003659.

Okumura T., Kawagucci S., Saito Y., Matsui Y., Takai K. and Imachi H. (2016) Hydrogen and carbon isotope systematics in hydrogenotrophic methanogenesis under H_2-limited and H_2-enriched conditions: implications for the origin of methane and its isotopic diagnosis. *Prog. Earth Planet. Sci.* **3**. https://doi.org/10.1186/s40645-40016-40088-40643.

Onstott T. C., Lin L.-H., Davidson M., Mislowack B., Borcsik M., Hall J., Slater G., Ward J., Sherwood Lollar B., Lippmann-Pipke J., Boice E., Pratt L. M., Pfiffner S., Moser D., Gihring T., Kieft T. L., Phelps T. J., Vanheerden E., Litthaur D., Deflaun M., Rothmel R., Wanger G. and Southam G. (2006) The origin and age of biogeochemical trends in deep fracture water of the Witwatersrand Basin, South Africa. *Geomicrobiol. J.* **23**, 369–414.

Orcutt B. N., Sylvan J. B., Knab N. J. and Edwards K. J. (2011) Microbial ecology of the dark ocean above, at, and below the seafloor. *Microbiol. Mol. Biol. Rev.* **75**, 361–422.

Palmer D. A. and Drummond S. E. (1986) Thermal decarboxylation of acetate. Part I. The kinetics and mechanism of reaction in aqueous solution. *Geochim. Cosmochim. Acta* **50**, 813–823.

Pester N. J., Ding K. and Seyfried, Jr., W. E. (2014) Magmatic eruptions and iron volatility in deep-sea hydrothermal fluids. *Geology* **42**, 255–258.

Pester N. J., Rough M., Ding K. and Seyfried, Jr., W. E. (2011) A new Fe/Mn geothermometer for hydrothermal systems: implications for high-salinity fluids at 13°N on the East Pacific Rise. *Geochim. Cosmochim. Acta* **75**, 7881–7892.

Pester N. J., Butterfield D. A., Foustoukos D. I., Roe K. K., Ding K., Shank T. M. and Seyfried, Jr., W. E. (2008) The chemistry of diffuse-flow vent fluids on the Galapagos Rift (86°W): Temporal variability and subseafloor phase equilibria controls. In *Magma to Microbe: Modeling Hydrothermal Processes at Oceanic Spreading Centers, Geophys. Monogr. Ser., 178* (eds. R. P. Lowell, J. S. Seewald, M. R. Perfit and A. Metaxas). AGU, Washington, D.C., pp. 123–144.

Proskurowski G., Lilley M. D., Kelley D. S. and Olson E. J. (2006) Low temperature volatile production at the Lost City Hydrothermal Field, evidence from a hydrogen stable isotope geothermometer. *Chem. Geol.* **229**, 331–343.

Reeves E. P., Seewald J. S. and Sylva S. P. (2012) Hydrogen isotope exchange between *n*-alkanes and water under hydrothermal conditions. *Geochim. Cosmochim. Acta* **77**, 582–599.

Reeves E. P., Seewald J. S., Saccocia P. J., Bach W., Craddock P. R., Shanks W. C., Sylva S. P., Walsh E., Pichler T. and Rosner M. (2011) Geochemistry of hydrothermal fluids from the PACMANUS, Northeast Pual and Vienna Woods hydrothermal fields, Manus Basin, Papua New Guinea. *Geochim. Cosmochim. Acta* **75**, 1088–1123.

Reysenbach A.-L., Liu Y., Banta A. B., Beveridge T. J., Kirshtein J. D., Schouten S., Tivey M. K., Von Damm K. L. and Voytek M. A. (2006) A ubiquitous thermoacidophillic archaeon from deep-sea hydrothermal vents. *Nature* **442**, 444–447.

Richet P., Bottinga Y. and Javoy M. (1977) A review of hydrogen, carbon, nitrogen, oxygen, sulphur, and chlorine stable isotope fractionation among gaseous molecules. *Annu. Rev. Earth Planet. Sci.* **5**, 65–110.

Robert F., Gautier D. and Dubrulle B. (2000) The solar system D/H ratio: observations and theories. *Space Sci. Rev.* **92**, 201–224.

Romanek C. S., Zhang C. L., Li Y., Horita J., Vali H., Cole D. R. and Phelps T. J. (2003) Carbon and hydrogen isotope fractionations associated with dissimilatory iron-reducing bacteria. *Chem. Geol.* **195**, 5–16.

Roy L. P. (1962) Influence of temperature on the electrolytic separation factor of hydrogen isotopes. *Can. J. Chem.* **40**, 1452–1460.

Schmidt K., Koschinsky A., Garbe-Schonberg D., de Carvalho L. M. and Seifert R. (2007) Geochemistry of hydrothermal fluids from the ultramafic-hosted Logatchev hydrothermal field, 15°N on the Mid-Atlantic Ridge: temporal and spatial investigation. *Chem. Geol.* **242**, 1–21.

Schrenk M. O., Kelley D. S., Bolton S. A. and Baross J. A. (2004) Low archaeal diversity linked to subseafloor geochemical processes at the Lost City Hydrothermal Field, Mid-Atlantic Ridge. *Environ. Microbiol.* **6**, 1086–1095.

Scott S., Driesner T. and Weis P. (2015) Geologic controls on supercritical geothermal resources above magmatic intrusions. *Nat. Comm.* **6**, 7837, doi: 7810.1038/ncomms8837.

Scott S., Gunnarsson I., Arnórsson S. and Stefánsson A. (2014) Gas chemistry, boiling and phase segregation in a geothermal system, Hellisheidi, Iceland. *Geochim. Cosmochim. Acta* **124**, 170–189.

Seewald J. S. and Seyfried, Jr., W. E. (1990) The effect of temperature on metal mobility in subseafloor hydrothermal systems: constraints from basalt alteration experiments. *Earth Planet. Sci. Lett.* **101**, 388–403.

Seewald J., Cruse A. and Saccocia P. (2003) Aqueous volatiles in hydrothermal fluids from the Main Endeavour Field, northern Juan de Fuca Ridge: temporal variability following earthquake activity. *Earth Planet. Sci. Lett.* **216**, 575–590.

Seward T. M. and Kishima N. (1987) Problems in working with hydrogen under hydrothermal. In *Hydrothermal Experimental Techniques* (eds. G. C. Ulmer and H. L. Barnes). Wiley Interscience, pp. 141–156.

Seyfried, Jr., W. E. (1987) Experimental and theoretical constraints on hydrothermal alteration processes at mid-ocean ridges. *Annu. Rev. Earth Planet. Sci.* **15**, 317–335.

Seyfried, Jr., W. E. and Ding K. (1995) Phase equilibria in subseafloor hydrothermal systems: a review of the role of redox, temperature, pH and dissolved Cl on the chemistry of hot spring fluids at mid-ocean ridges. In *Seafloor Hydrothermal Systems: Physical, Chemical, Biological and Geological Interactions, Geophys. Monogr. Ser., 91* (eds. S. E. Humphris, R. A. Zierenberg, L. S. Mullineaux and R. E. Thompson). AGU, Washington, D.C., pp. 248–273.

Seyfried, Jr., W. E., Gordon P. C. and Dickson F. W. (1979) A new reaction cell for hydrothermal solution equipment. *Am. Mineral.* **64**, 646–649.

Seyfried, Jr., W. E., Janecky D. R. and Berndt M. E. (1987) Rocking autoclaves for hydrothermal experiments II: the flexible reaction-cell system. In *Hydrothermal Experimental*

Techniques (eds. G. C. Ulmer and H. L. Barnes). Wiley Interscience, pp. 216–239.

Seyfried, Jr., W. E., Ding K. and Berndt M. E. (1991) Phase equilibria constraints on the chemistry of hot spring fluids at mid-ocean ridges. *Geochim. Cosmochim. Acta* **55**, 3559–3580.

Seyfried, Jr., W. E., Foustoukos D. I. and Fu Q. (2007) Redox evolution and mass transfer during serpentinization: an experimental and theoretical study at 200°C, 500 bar with implications for ultramafic-hosted hydrothermal systems at mid-ocean ridges. *Geochim. Cosmochim. Acta* **71**, 3872–3886.

Seyfried, Jr., W. E., Pester N. and Qi F. (2010) Phase equilibria controls on the chemistry of vent fluids from hydrothermal systems on slow spreading ridges: reactivity of plagioclase and olivine solid solutions and the pH-silica connection. In *Diversity of Hydrothermal Systems on Slow Spreading Ocean Ridges, Geophys. Monogr. Ser. 188* (eds. P. A. Rona, C. W. Devey, J. Dyment and B. J. Murton). AGU, Washington, D.C., pp. 297–320.

Seyfried, Jr., W. E., Pester N. J., Ding K. and Rough M. (2011) Vent fluid chemistry of the Rainbow hydrothermal system (36° N, MAR): phase equilibria and in-situ pH controls on subseafloor alteration processes. *Geochim. Cosmochim. Acta* **75**, 1574–1593.

Seyfried, Jr., W. E., Pester N. J., Tutolo B. M. and Ding K. (2015) The Lost City hydrothermal system: constraints imposed by vent fluid chemistry and reaction path models on subseafloor heat and mass transfer processes. *Geochim. Cosmochim. Acta* **163**, 59–79.

Shanks, III, W. C. (2001) Stable isotopes in seafloor hydrothermal systems: vent fluids, hydrothermal deposits, hydrothermal alteration, and microbial processes. In *Stable Isotope Geochemistry, Rev. Mineral. Geochem.* (eds. J. W. Valley and D. R. Cole). MSA, pp. 469–526.

Sheppard D. S., Truesdell A. H. and Janik C. J. (1992) Geothermal gas compositions in Yellowstone National Park, USA. *J. Volcanol. Geoth. Res.* **51**, 79–93.

Sherwood Lollar B., Frape S. K., Fritz P., Macko S. A., Welhan J. A., Blomqvist R. and Lahermo P. W. (1993a) Evidence for bacterially generated hydrocarbon gas in Canadian shield and fennoscandian shield rocks. *Geochim. Cosmochim. Acta* **57**, 5073–5085.

Sherwood Lollar B., Frape S. K., Weise S. M., Fritz P., Macko S. A. and Welhan J. A. (1993b) Abiogenic methanogenesis in crystalline rocks. *Geochim. Cosmochim. Acta* **57**, 5087–5097.

Sherwood Lollar B., Lacrampe-Couloume G., Voglesonger K., Onstott T. C., Pratt L. M. and Slater G. F. (2008) Isotopic signatures of CH_4 and higher hydrocarbon gases from Precambrian Shield sites: a model for abiogenic polymerization of hydrocarbons. *Geochim. Cosmochim. Acta* **72**, 4778–4795.

Sherwood Lollar B., Voglesonger K., Lin L.-H., Lacrampe-Couloume G., Telling J., Abrajano T. A., Onstott T. C. and Pratt L. M. (2007) Hydrogeologic controls on episodic H_2 release from precambrian fractured rocks—energy for deep subsurface life on Earth and Mars. *Astrobiology* **7**, 971–986.

Shock E. L. (1992) Chemical environments of submarine hydrothermal systems. *Origins Life Evol. Biosphere* **22**, 67–107.

Simmons S. F., Harris S. P. and Cassidy J. (2005) Lake-filled depressions resulting from cold gas discharge in the Ngawha Geothermal Field, New Zealand. *J. Volcanol. Geoth. Res.* **147**, 329–341.

Simmons S. F., Brown K. L. and Tutolo B. M. (2016) Hydrothermal transport of Ag, Au, Cu, Pb, Te, Zn, and other metals and metalloids in New Zealand geothermal systems: Spatial patterns, fluid-mineral equilibria, and implications for epithermal mineralization. *Econ. Geol.* **111**, 589–618.

Sleep N. H., Meibom A., Fridriksson T., Coleman R. G. and Bird D. K. (2004) H_2-rich fluids from serpentinization: geochemical and biotic implications. *Proc. Natl. Acad. Sci. USA* **101**, 12818–12823.

Spycher N. F. and Reed M. H. (1988) Fugacity coefficients of H_2, CO_2, CH_4, H_2O and of H_2O-CO_2-CH_4 mixtures: a virial equation treatment for moderate pressures and temperatures applicable to calculations of hydrothermal boiling. *Geochim. Cosmochim. Acta* **52**, 739–749.

Stojić D. L., Miljanić Š. S., Grozdić T. D., Golobočanin D. D., Sovili S. P. and Jakšić M. M. (1994) D/H isotope separation efficiency in water electrolysis. Improvement by in situ activation at different temperatures. *Int. J. Hydrogen Energy* **19**, 587–590.

Strauss H. L., Chen Z. and Loong C.-K. (1994) The diffusion of H_2 in hexagonal ice at low temperatures. *J. Chem. Phys.* **101**, 7177–7180.

Suda K., Ueno Y., Yoshizaki M., Nakamura H., Kurokawa K., Nishiyama E., Yoshino K., Hongoh Y., Kawachi K., Omori S., Yamada K., Yoshida N. and Maruyama S. (2014) Origin of methane in serpentinite-hosted hydrothermal systems: the CH_4–H_2–H_2O hydrogen isotope systematics of the Hakuba Happo hot spring. *Earth Planet. Sci. Lett.* **386**, 112–125.

Suess H. E. (1949) Das Gleichgewicht $H_2 + HDO \rightleftharpoons HD+H_2O$ und die weiteren austauschgleichgewichte im system H_2, D_2 und H_2O. *Z. Naturforsch.* **4**, 328–332.

Symons E. A. and Buncel E. (1973) Base-catalyzed isotopic exchange of molecular hydrogen. II. Rate dependence on basicity in the dimethyl sulfoxide-water system. *Can. J. Chem.* **51**, 1673–1681.

Taran Y. A., Pilipenko V. P., Rozhkov A. M. and Vakin E. A. (1992) A geochemical model for fumaroles of the Mutnovsky volcano, Kamchatka, USSR. *J. Volcanol. Geoth. Res.* **49**, 269–283.

Taran Y. A., Varley N. R., Inguaggiato S. and Cienfuegos E. (2010) Geochemistry of H_2- and CH_4-enriched hydrothermal fluids of Socorro Island, Revillagigedo Archipelago, Mexico. Evidence for serpentinization and abiogenic methane. *Geofluids* **10**, 542–555.

Titarenko S. S. and McCaig A. M. (2016) Modelling the Lost City hydrothermal field: influence of topography and permeability structure. *Geofluids* **16**, 314–328.

Tivey M. K., Olson L. O., Miller V. W. and Light R. D. (1990) Temperature measurements during initiation and growth of a black smoker chimney. *Nature* **346**, 51–54.

Tobias H. J., Goodman K. J., Blacken C. E. and Brenna J. T. (1995) High-precision D/H measurement from hydrogen gas and water by continuous-flow isotope ratio mass spectrometry. *Anal. Chem.* **67**, 2486–2492.

Toki, T., Maegawa, K., Tsunogai, U., Kawagucci, S., Takahata, N., Sano, Y., Ashi, J., Kinoshita, M., Gamo, T., 2011. Gas chemistry of pore fluids from Oomine Ridge on the Nankai accretionary prism. In: Ogawa, Y., Anma, R., Dilek, Y. (Eds.), Accretionary Prisms and Convergent Margin Tectonics in the Northwest Pacific Basin, Mod. Appr. Sol. Earth Sci. vol. 8, pp. 247–262.

Topley B. and Eyring H. (1934) The separation of the hydrogen isotopes by electrolysis. Part I. *J. Chem. Phys.* **2**, 217–230.

Truesdell A. H., Nathenson M. and Rye R. O. (1977) The effects of subsurface boiling and dilution on the isotopic compositions of Yellowstone thermal waters. *J. Geophys. Res.* **82**, 3694–3704.

Tsunogai U., Kamimura K., Anzai S., Nakagawa F. and Komatsu D. D. (2011) Hydrogen isotopes in volcanic plumes: tracers for remote temperature sensing of fumaroles. *Geochim. Cosmochim. Acta* **75**, 4531–4546.

Vacquand C., Deville E., Beaumont V., Guyot F., Sissmann O., Pillot D., Arcilla C. and Prinzhofer A. (2018) Reduced gas seepages in ophiolitic complexes: evidences for multiple origins of the H2-CH4-N2 gas mixtures. *Geochim. Cosmochim. Acta* **223**, 437–461.

Valentine D. L., Chidthaisong A., Rice A., Reeburgh W. S. and Tyler S. C. (2004) Carbon and hydrogen isotope fractionation by moderately thermophilic methanogens. *Geochim. Cosmochim. Acta* **68**, 1571–1590.

Vignais P. M. and Billoud B. (2007) Occurrence, classification, and biological function of hydrogenases: an overview. *Chem. Rev.* **107**, 4206–4272.

Von Damm K. L. (2000) Chemistry of hydrothermal vent fluids from 9°-10°N, East Pacific Rise: "Time zero," the immediate posteruptive period. *J. Geophys. Res.* **105**, 11203–11222.

Von Damm K. L. and Lilley M. D. (2004) Diffuse flow hydrothermal fluids from 9°50'N East Pacific Rise: origin, evolution and biogeochemical controls. In *The Subseafloor Biosphere at Mid-Ocean Ridges, Geophys. Monogr. Ser.* (eds. W. S. Wilcock, C. Cary, E. De Long, D. Kelley and J. Barross). AGU, Washington, D.C., pp. 245–268.

Von Damm K. L., Edmond J. M., Grant B., Measures C. I., Walden B. and Weiss R. F. (1985) Chemistry of submarine hydrothermal solutions at 21°N, East Pacific Rise. *Geochim. Cosmochim. Acta* **49**, 2197–2220.

Waite J. H., Glein C. R., Perryman R. S., Teolis B. D., Magee B. A., Miller G., Grimes J., Perry M. E., Miller K. E., Bouquet A., Lunine J. I., Brockwell T. and Bolton S. J. (2017) Cassini finds molecular hydrogen in the Enceladus plume: evidence for hydrothermal processes. *Science* **356**, 155–159.

Waite, Jr., J. H., Lewis W. S., Magee B. A., Lunine J. I., McKinnon W. B., Glein C. R., Mousis O., Young D. T., Brockwell T., Westlake J., Nguyen M. J., Teolis B. D., Niemann H. B., McNutt, Jr, R. L., Perry M. and Ip W. H. (2009) Liquid water on Enceladus from observations of ammonia and ^{40}Ar in the plume. *Nature* **460**, 487–490.

Walter S., Laukenmann S., Stams A. J. M., Vollmer M. K., Gleixner G. and Röckmann T. (2012) The stable isotopic signature of biologically produced molecular hydrogen (H_2). *Biogeosciences* **9**, 4115–4123.

Wanner C., Peiffer L., Sonnenthal E., Spycher N., Iovenitti J. and Kennedy B. M. (2014) Reactive transport modeling of the Dixie Valley geothermal area: insights on flow and geothermometry. *Geothermics* **51**, 130–141.

Welhan J. A. (1981) *Carbon and Hydrogen Gases in Hydrothermal Systems: The Search for a Mantle Source* PhD thesis. UC San Diego.

Welhan J. A. and Craig H. (1983) Methane, hydrogen and helium in hydrothermal fluids at 21°N on the East Pacific Rise. In *Hydrothermal Processes at Seafloor Spreading Centers* (eds. P. A. Rona, K. Bostrom, L. Laubier and K. L. Smith). Plenum Press, pp. 391–409.

White D. E., Muffler L. J. P. and Truesdell A. H. (1971) Vapor-dominated hydrothermal systems compared with hot-water systems. *Econ. Geol.* **66**, 75–97.

Wilcock W. S. D. (2004) Physical response of mid-ocean ridge hydrothermal systems to local earthquakes. *Geochem. Geophys. Geosyst.* **5**, Q110099. https://doi.org/10.1029/2004GC000701.

Wilmarth W. K., Dayton J. C. and Flournoy J. M. (1953) The mechanism of exchange of hydrogen gas and aqueous alkali. *J. Am. Chem. Soc.* **75**, 4549–4553.

Yang H., Gandhi H., Shi L., Kreuzer H. W., Ostrom N. E. and Hegg E. L. (2012) Using gas chromatography/isotope ratio mass spectrometry to determine the fractionation factor for H_2 production by hydrogenases. *Rapid Commun. Mass Spectrom.* **26**, 61–68.

Yuce G., Italiano F., D'Alessandro W., Yalcin T. H., Yasin D. U., Gulbay A. H., Ozyurt N. N., Rojay B., Karabacak V., Bellomo S., Brusca L., Yang T., Fu C. C., Lai C. W., Ozacar A. and Walia V. (2014) Origin and interactions of fluids circulating over the Amik Basin (Hatay, Turkey) and relationships with the hydrologic, geologic and tectonic settings. *Chem. Geol.* **388**, 23–39.

Associate editor: Matthew S. Fantle

Kinetics of D/H isotope fractionation between molecular hydrogen and water

AUTHORS: N. J. PESTER[1, 2*], M. E. CONRAD[1], K. G. KNAUSS[1], D. J. DEPAOLO[1, 2]

[1]Earth and Environmental Sciences, Lawrence Berkeley National Laboratory, Berkeley, CA 94720, USA

[2]Department of Earth and Planetary Science, University of California, Berkeley, CA 94720, USA

*corresponding email: njpester@lbl.gov

This file contains **Supplementary Information** to the above publication
in *Geochimica et Cosmochimica Acta*

METHOD:

New polynomial regressions for equilibrium D/H isotope fractionation in the system H_2–H_2O ($\alpha_{H2O\text{-}H2(eq)}$).

I. Variables

Here we develop three new polynomial regressions for equilibrium D/H isotope fractionation that account for the phase state(s) of the system H_2–H_2O. The D/H isotope ratios associated with species components and their phase states are designated as:

liquid H_2O: $[D/H]_{H2O(liq)}$

H_2O vapor/gas: $[D/H]_{H2O(vap)}$

gaseous H_2: $[D/H]_{H2(gas)}$

dissolved H_2: $[D/H]_{H2(aq)}$

Equilibrium liquid/vapor isotope fractionation factors are defined as:

$$\alpha_{H2O(L\text{-}V)} = [D/H]_{H2O(liq)} / [D/H]_{H2O(vap)} \text{ and } \alpha_{H2(L\text{-}V)} = [D/H]_{H2(aq)} / [D/H]_{H2(gas)}$$

Equilibrium H_2O-H_2 fractionation factors are defined as:

$$\alpha_{H2O(v)\text{-}H2(g)} = [D/H]_{H2O(vap)} / [D/H]_{H2(gas)} \text{ and } \alpha_{H2O(L)\text{-}H2(AQ)} = [D/H]_{H2O(liq)} / [D/H]_{H2(aq)}$$

An additional H_2–H_2O fractionation factor is commonly used (see section 4.2, main text), which inherently implies all four components coexist at equilibrium. This alpha we define as:

$$\alpha_{H2O(L)\text{-}H2(g)} = [D/H]_{H2O(liq)} / [D/H]_{H2(gas)} = \alpha_{H2O(v)\text{-}H2(g)} * \alpha_{H2O(L\text{-}V)}$$

II. Alpha regressions

In the following sections, using the best currently available data, we regress equilibrium curves to represent $\alpha_{H2O(v)-H2(g)}$, $\alpha_{H2O(L)-H2(AQ)}$ and $\alpha_{H2O(L)-H2(g)}$ with internal consistency. We first treat $\alpha_{H2O(v)-H2(g)}$, then use $\alpha_{H2O(v)-H2(g)}$ and $\alpha_{H2O(L-V)}$ to regress a curve for $\alpha_{H2O(L)-H2(g)}$. Finally, in conjunction with the new $\alpha_{H2O(L)-H2(g)}$ and $\alpha_{H2O(v)-H2(g)}$ curves, both the new data presented here, and previously reported data for $\alpha_{H2(L-V)}$, are used to define a representative curve for $\alpha_{H2O(L)-H2(AQ)}$.

1) $\alpha_{H2O(v)-H2(g)} = [D/H]_{H2O(vap)} / [D/H]_{H2(gas)}$

For regression of $\alpha_{H2O(v)-H2(g)}$ (Fig. S1) we use the experimental data of Suess (1949) and Fu et al. (2007), and the theoretical calculations of Bardo and Wolfsberg (1976). The data of Fu et al. (2007), representing a supercritical liquid (400 °C, 500 bars) rather than a gas/vapor, were still considered a valuable constraint because they are reproducible (3 points) and consistent with currently available $\alpha_{H2O(v)-H2(g)}$ models. Ultimately, the regressions we produce here assume no meaningful difference in $\alpha_{H2O-H2(eq)}$ associated with P for $T > 374$ °C (the H_2O critical point). Raw data rather than averages were used for the experimental data in order to give weight to reproducibility. The theoretical calculations of Bardo and Wolfsberg (1976) show good agreement with the experimental data of Suess (1949). We follow Horibe and Craig (1995) in valuing the more rigorous data of Bardo and Wolfsberg (1976) above other theoretical relationships, and include these data in the regression, calculated in increments of 20 °C between 0 and 200 °C.

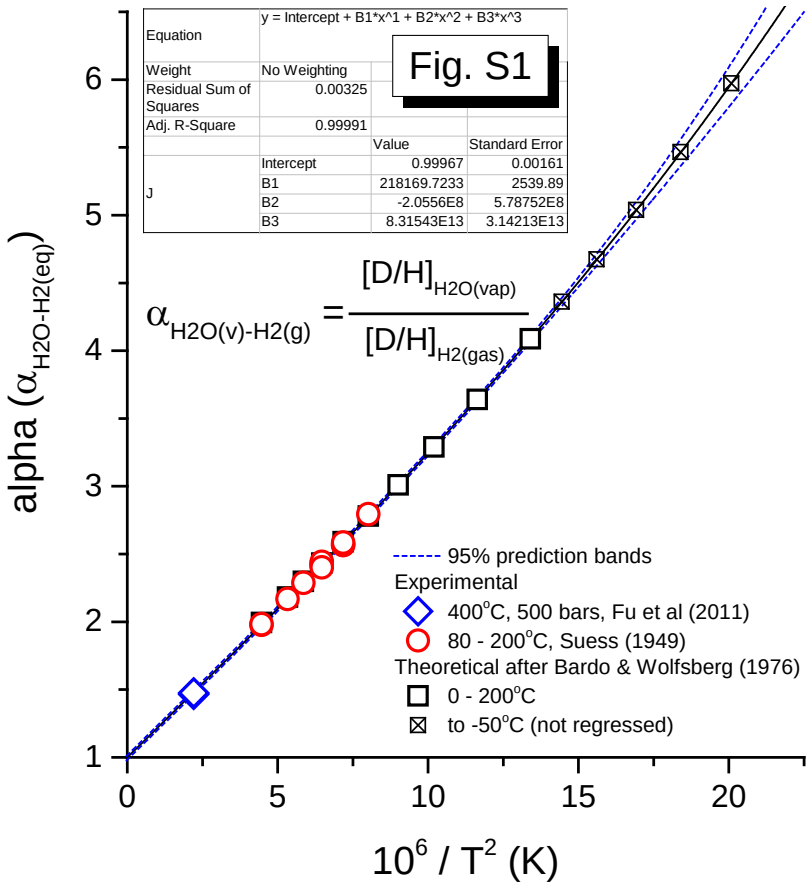

The temperature dependence of alpha may be best represented as $1/T$ or $1/T^2$ with either a 2nd, 3rd or 4th order polynomial, considering the system and the temperature range (Criss, 1999). Preliminary regressions of the data shown in Fig. S1 indicated a 3rd order regression of $1/T^2$ best represents $\alpha_{H2O\text{-}H2(eq)}$, based on the correlation coefficients and the observation that the curve naturally extrapolated to $\alpha \approx 1$ at infinite T, consistent with theoretical predictions. The final regression, shown in Fig. S1, also included a data point at (0, 1) to help reinforce this theoretically predicted behavior. Although not included in the regression, additional calculations after Bardo and Wolfsberg (1976) are shown for subzero (°C) temperatures. Ultimately, there is little practical difference between $\alpha_{H2O(v)\text{-}H2(g)}$ values calculated using the regression presented here relative to those calculated with the relationship given by Bardo and Wolfsberg (1976). However, divergence occurs for the latter at extreme temperatures (T < -150 °C and T > 1000 °C) facilitated by their 4th order representation.

2) $\alpha_{H2O(L)\text{-}H2(g)}$ = $[D/H]_{H2O(liq)}$ / $[D/H]_{H2(gas)}$

A regression of $\alpha_{H2O(L)\text{-}H2(g)}$ is shown in Fig. S2. This alpha implies the coexistence of vapor- and liquid-phase H_2O. Therefore, $\alpha_{H2O(L)\text{-}H2(g)}$ is moot at both subzero (°C) and supercritical temperatures. Values of $\alpha_{H2O(L)\text{-}H2(g)}$ were calculated from $\alpha_{H2O(v)\text{-}H2(g)}$ * $\alpha_{H2O(L\text{-}V)}$ for T increments of 20 °C between 0 and 360 °C, as well as 373 °C, using the relationship in Fig. S1 and $\alpha_{H2O(L\text{-}V)}$ values calculated after Horita and Wesolowski (1994). Derivation of these $\alpha_{H2O(L)\text{-}H2(g)}$ values is therefore similar to those given by Horibe and Craig (1995). Although not included in the regression, the experimental data of Rolston et al. (1976) show good agreement (Fig. S2). The primary reason we have regressed an independent representation of $\alpha_{H2O(L)\text{-}H2(g)}$ is to facilitate calculating internally consistent values of $\alpha_{H2O(L)\text{-}H2(AQ)}$ using currently available data for $\alpha_{H2(L\text{-}V)}$ (see below).

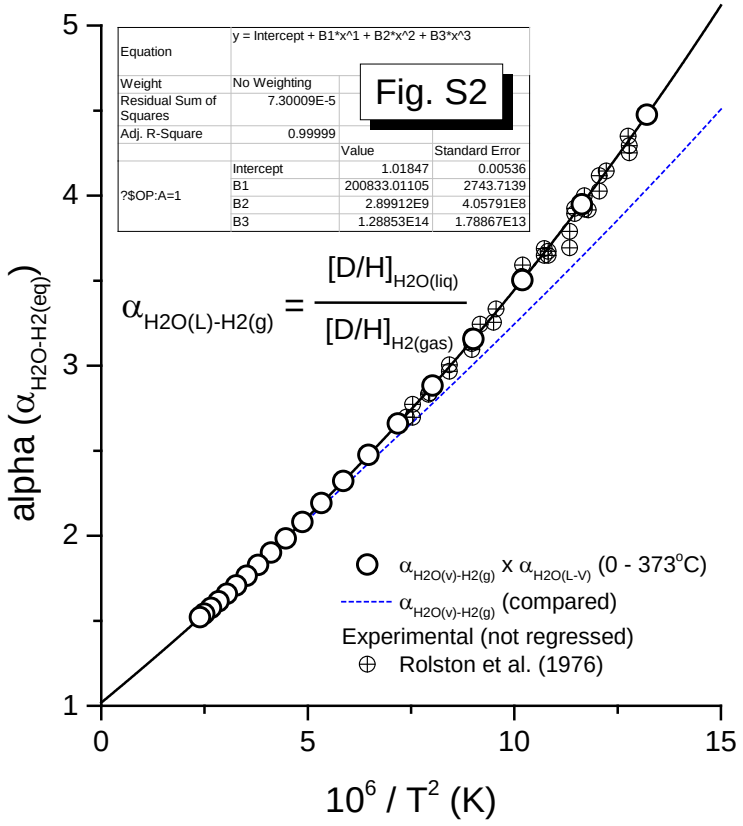

3) $\alpha_{H2O(L)-H2(AQ)} = [D/H]_{H2O(liq)} / [D/H]_{H2(aq)}$

Relatively few data exist with which to constrain $\alpha_{H2O(L)-H2(AQ)}$, including the new experimental data presented here (at 97, 54 and 22 °C). First, given $\alpha_{H2O(v)-H2(g)}$ and $\alpha_{H2O(L)-H2(g)}$ converge for T > ~220 °C (Fig. S2), we can reasonably assume $\alpha_{H2O(L)-H2(AQ)} = \alpha_{H2O(v)-H2(g)}$ for higher temperatures, and we therefore used $\alpha_{H2O(v)-H2(g)}$ values calculated at 20 °C increments between 260 and 1000 °C to "anchor" the regression. For lower T, we could not find any other studies in which $\alpha_{H2O(L)-H2(AQ)}$ is reported. However, if only our (3) data points were to be included in the regression, there is concern associated with the relatively high uncertainty of the 22 °C alpha. Recognizing that $\alpha_{H2O(L)-H2(g)} / \alpha_{H2(L-V)} = \alpha_{H2O(L)-H2(AQ)}$, we evaluated currently available data for $\alpha_{H2(L-V)}$ in order to provide additional constraints. As part of an experimental study of kinetic isotope fractionation during gas-liquid exchange, Knox et al. (1992) determined $\alpha_{H2(L-V)}$ at 21 °C using two different approaches, where the δD_{H2} of coexisting gas and $H_{2(aq)}$ were both directly measured. These two experiments gave a reproducible value of $\alpha_{H2(L-V)} = 1.037$, which translates to $\alpha_{H2O(L)-H2(AQ)} = 3.786$, and compares favorably to our 22 °C value of $\alpha_{H2O(L)-H2(AQ)} = 3.814 \pm 0.070$ (2σ) (Figs. 7, S3).

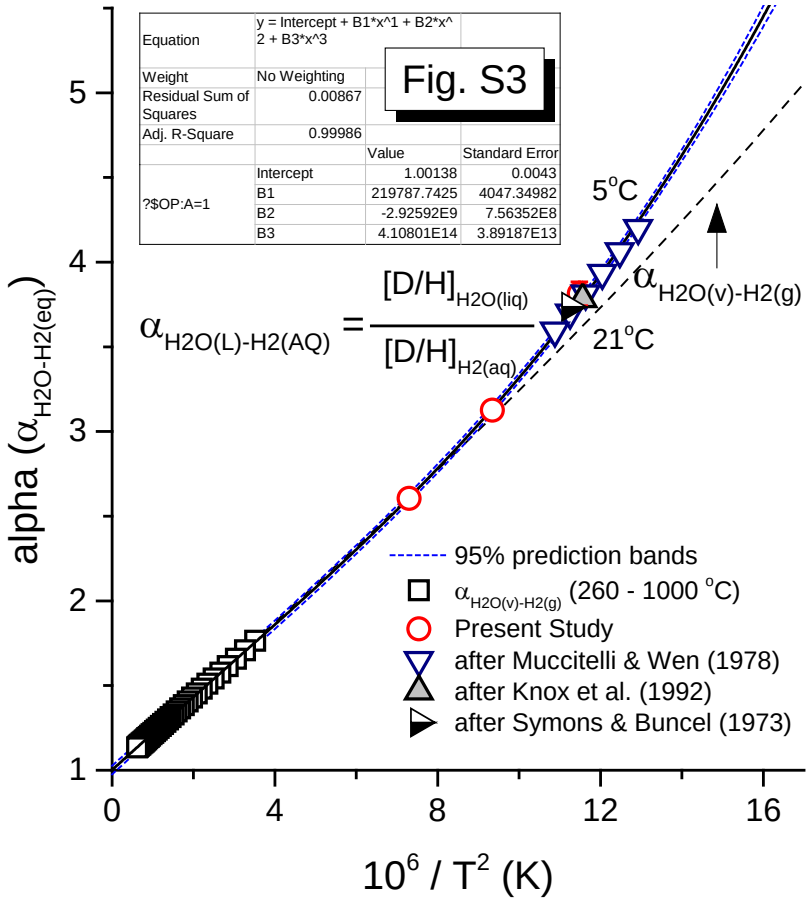

Additional $\alpha_{H2(L-V)}$ data were derived from Symons and Buncel (1973) and Muccitelli and Wen (1978). These studies report data on the solubility of D_2 gas in H_2O, which may be used with known solubilities of H_2 gas in order to derive $\alpha_{H2(L-V)}$ values (Jancsó, 2002; Muccitelli and Wen, 1978). For example, Muccitelli and Wen (1978) report alpha values based on the ratio of the Henry's constants (k_H) of D_2 and H_2 gases between 5 and 30 °C. However, for natural systems, D_2 gas will be a negligible

component, which necessitates comparing the relative solubilities of HD and H_2 gases under the assumption that the k_H for HD gas may be represented by the average of those for H_2 gas and D_2 gas. We note that the raw rather than the smoothed k_H values reported for D_2 by Muccitelli and Wen (1978) were used for the calculations herein. This equates (within uncertainty) to using the square root of the alpha values reported by Muccitelli and Wen (1978) as the $\alpha_{H2(L-V)}$ of interest. Although there is more uncertainty associated with $\alpha_{H2(L-V)}$ values derived using isotope solubility effects (e.g., compared to the more direct measurements of Knox et al. (1992)), the calculated $\alpha_{H2O(L)-H2(AQ)}$ values nonetheless show reasonable agreement for similar temperatures. The final $\alpha_{H2O(L)-H2(AQ)}$ regression includes all data shown in Fig. S3, where our 97 and 54 °C data points are weighted in triplicate in order to avoid favoring the higher uncertainty (but more numerous) lower *T* data. Conversely, no weighting was placed on any data for *T* < 54 °C because estimates of uncertainty are generally high (Fig. 7, see also Fig. S5 below) and difficult to meaningfully account for in a relative manner given the varied assumptions used in deriving $\alpha_{H2O(L)-H2(AQ)}$ from $\alpha_{H2(L-V)}$ values. Residuals of the fits for $\alpha_{H2O(v)-H2(g)}$ (Fig. S1) and $\alpha_{H2O(L)-H2(AQ)}$ (Fig. S3), along with the associated 95% confidence and 95% prediction limits, are compared in Fig. S4 below for *T* < 425 °C.

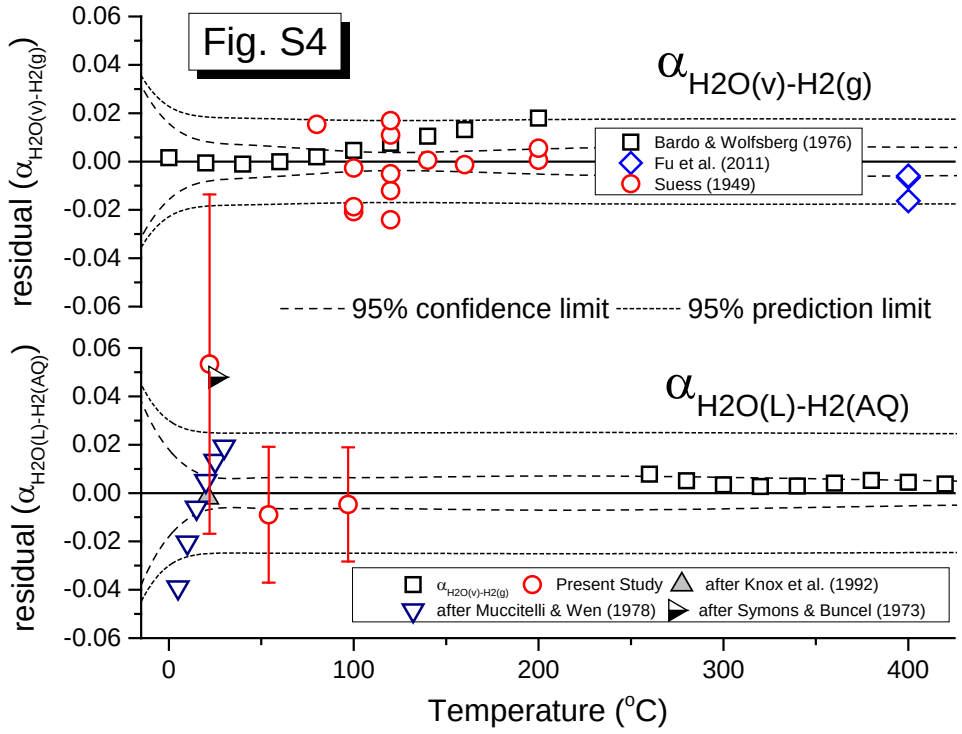

The range of the residuals for the experimental data constraining $\alpha_{H2O(L)-H2(AQ)}$ for *T* < 54 °C spans ~ ± 0.05, which is comparable to the estimated uncertainty of these data (exemplified by our 22 °C data point), but greater than the 95% prediction limit of ± 0.025 for *T* > 10 °C (Fig. S4). It is interesting to note that if all of these $\alpha_{H2O(L)-H2(AQ)}$ data for *T* <54 °C are excluded from the regression (cf. Fig. S3), the resulting *T* dependence of $\alpha_{H2O(L)-H2(AQ)}$ still falls within the 95% prediction limit of the relationship given in Fig. S3 (also Table 2).

Another way to evaluate the effect of including the indirectly calculated low-*T* data (Knox et al., 1992; Muccitelli and Wen, 1978; Symons and Buncel, 1973) on the *T* dependence of $\alpha_{H2O(L)-H2(AQ)}$ is to

consider the *T* dependence of $\alpha_{H2(L-V)}$ if back-calculated using the new $\alpha_{H2O(L)-H2(AQ)}$ and $\alpha_{H2O(L)-H2(g)}$ regressions (i.e. $\alpha_{H2(L-V)} = \alpha_{H2O(L)-H2(g)} / \alpha_{H2O(L)-H2(AQ)}$, Fig. S5 below). First, $\alpha_{H2(L-V)}$ converges to ~unity at the H_2O critical point (374 °C, star symbol, Fig. S5), which is requisite for vapor-liquid fractionation. The $\alpha_{H2(L-V)}$ trend generally exhibits a normal (i.e. expected) isotope effect, where $\alpha_{H2(L-V)}$ increases with decreasing *T* (cf. $\alpha_{H2O(L-V)}$, dash-dot curve), but the curve turns over slightly at ~40 °C. Within uncertainty of the data (Fig. S5) this would suggest that $\alpha_{H2(L-V)}$ effectively "levels off" between 1.03 and 1.04 for $T <$ 100 °C. This may be reasonable if the relative aqueous solubilities of H_2 and D_2 (or HD) do not actually change appreciably with *T* at these lower temperatures. Although not necessarily comparable, the relative solubilities of H_2 and D_2 in non-polar solvents, and the relative aqueous solubilities of CH_4 and CD_4 both show statistically insignificant *T* dependence in the experimentally measured ranges of -25 °C < *T* < 35 °C and 15 °C < *T* < 50 °C, respectively (Bacsik et al., 2002; Cook et al., 1957; Costa Gomes and Grolier, 2001).

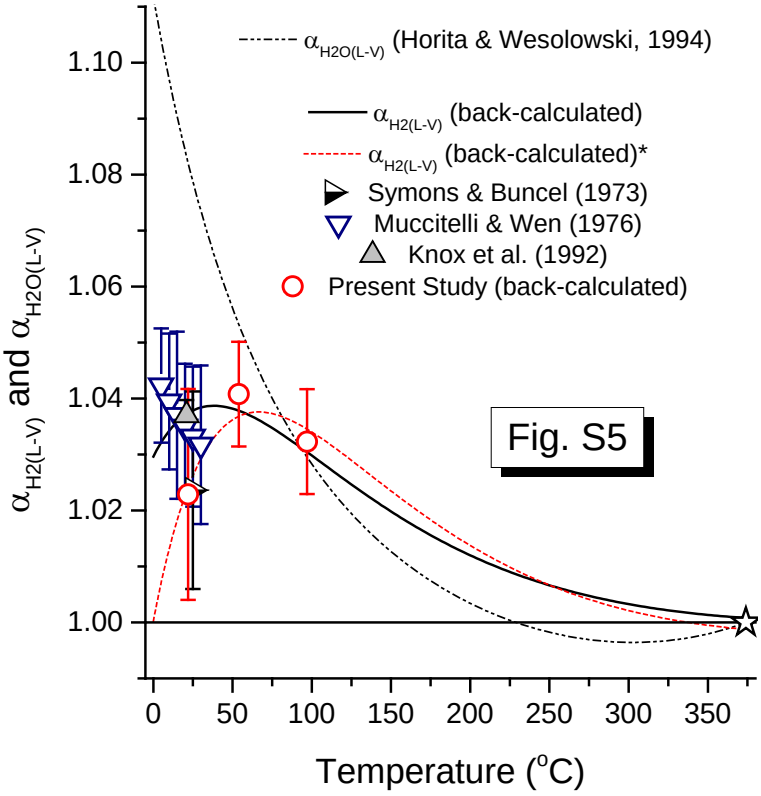

We performed an additional sensitivity exercise in which we regressed $\alpha_{H2O(L)-H2(AQ)}$ (cf. Fig. S3), but excluded all data for $T <$ 54 °C save our data point at 22 °C. In this case, the turnover in back-calculated $\alpha_{H2(L-V)}$ is more severe (*red dashed, Fig. S5), and the curve intersects unity at ~0 °C. This scenario seems less likely than the results observed when all the low-*T* data (< 54 °C) are included. Recalling also the above noted observation that the *T* dependence of $\alpha_{H2O(L)-H2(AQ)}$ (Fig. S3) is nearly equivalent when *all* the low-*T* data are excluded from the regression, this suggests the *T* vs. $\alpha_{H2O(L)-H2(AQ)}$ relationship given in Fig. S3 (also Table 2) is likely the most reasonable representation given currently available constraints.

REFERENCES

Bacsik, Z., Canongia Lopes, J.N., M. F. Costa Gomes, M.F., Jancsó, G., Mink, J., Pádua, A.A.H., 2002. Solubility isotope effects in aqueous solutions of methane. J. Chem. Phys. 116, 10816-10824.

Bardo, R.D., Wolfsberg, M., 1976. A theoretical calculation of the equilibrium constant for the isotopic exchange reaction between H_2O and HD. J. Phys. Chem. 80, 1068-1071.

Cook, M.W., Hanson, D.N., Alder, B.J., 1957. Solubility of hydrogen and deuterium in nonpolar Solvents. J. Chem. Phys. 26, 748-751.

Costa Gomes, M.F., Grolier, J.-P., 2001. Determination of Henry's law constants for aqueous solutions of tetradeuteriomethane between 285 and 325 K and calculation of the H/D isotope effect. Phys. Chem. Chem. Phys. 3, 1047-1052.

Criss, R.E., 1999. Principles of Stable Isotope Distribution. Oxford University Press.

Fu, Q., Lollar, B.S., Horita, J., Lacrampe-Couloume, G., Seyfried, W.E., Jr., 2007. Abiotic formation of hydrocarbons under hydrothermal conditions: Constraints from chemical and isotope data. Geochim. Cosmochim. Acta 71, 1982-1998.

Horibe, Y., Craig, H., 1995. D/H fractionation in the system methane-hydrogen-water. Geochim. Cosmochim. Acta 59, 5209-5217.

Horita, J., Wesolowski, D.J., 1994. Liquid-vapor fractionation of oxygen and hydrogen isotopes of water from the freezing to the critical temperature. Geochim. Cosmochim. Acta 58, 3425-3437.

Jancsó, G., 2002. Interpretation of isotope effects on the solubility of gases. Nukleonika 47, S53-S57.

Knox, M., Quay, P.D., Wilbur, D., 1992. Kinetic isotopic fractionation during air-water gas transfer of O_2, N_2, CH_4, and H_2. J. Geophys. Res. 97, 20335-20343.

Muccitelli, J., Wen, W.-Y., 1978. Solubilities of hydrogen and deuterium gases in water and their isotope fractionation factor. J. Sol. Chem. 7, 257-267.

Rolston, J.H., den Hartog, J., Butler, J.P., 1976. The deuterium isotope separation factor between hydrogen and liquid water. J. Phys. Chem. 80, 1064-1067.

Suess, H.E., 1949. Das Gleichgewicht $H_2 + HDO \rightleftharpoons HD+H_2O$ und die weiteren austauschgleichgewichte im system H_2, D_2 und H_2O. Z. Naturforsch. 4, 328-332.

Symons, E.A., Buncel, E., 1973. Base-catalyzed isotopic exchange of molecular hydrogen. II. Rate dependence on basicity in the dimethyl sulfoxide-water system. Can. J. Chem. 51, 1673-1681.